wisconsin astrophysics

THE HUBBLE SPACE TELESCOPE HIGH SPEED PHOTOMETER

NUMBER 659
SEPTEMBER 1997

R. C. BLESS, E. E. RICHARDS, *UNIVERSITY OF WISCONSIN-MADISON,*

J. F. DOLAN, *NASA GODDARD SPACE FLIGHT CENTER,*

J. L. ELLIOT, *MIT AND LOWELL OBSERVATORY,*

M. NELSON, *VATICAN OBSERVATORY RESEARCH GROUP, UNIVERSITY OF ARIZONA*

J. W. PERCIVAL, *UNIVERSITY OF WISCONSIN-MADISON*

E. L. ROBINSON, *UNIVERSITY OF TEXAS*

M. TAYLOR, *LORAS COLLEGE*

G. W. VAN CITTERS, *NATIONAL SCIENCE FOUNDATION*

R. L. WHITE, *SPACE TELESCOPE SCIENCE INSTITUTE*

THE HUBBLE SPACE TELESCOPE'S HIGH SPEED PHOTOMETER

R.C. Bless[1], E. E. Richards[1], J. F. Dolan[2], J. L. Elliot[3], M. Nelson[4], J.W. Percival[1], E. L. Robinson[5], M. Taylor[6], G. W. Van Citters[7], R. L. White[8]

[1]University of Wisconsin-Madison, [2] NASA Goddard Space Flight Center, [3]MIT and Lowell Observatory, [4]Vatican Observatory Research Group, University of Arizona, [5]University of Texas, [6]Loras College, [7]National Science Foundation, [8]Space Telescope Science Institute

ABSTRACT

We present an overview of the High Speed Photometer (HSP), one of the five original instruments on the Hubble Space Telescope (HST). As its name implies, the HSP was intended for precise high time resolution photometry from visual to ultraviolet wavelengths; sample times as short as 10.7 microseconds were possible. Three image dissectors-two with CsTe cathodes for the far UV and one with a bialkali cathode sensitive to the near UV and visible spectral region-were used for photometry of stars and galaxies. Twenty-three different broad- and narrow-band filters spanning the spectral range from 1200 to 7500 A provided a variety of spectral band passes. A beam splitter passed blue light to one of the image dissectors and red light to a photomultiplier with a GaAs cathode, allowing simultaneous observations to be made in these two spectral bands (in particular, planetary occultations). A fourth image dissector (bialkali cathode) with associated polarization analyzers allowed the measurement of broad-band linear polarization at near-ultraviolet wavelengths. Except for an instability in the sensitivity of the VIS image dissector, the instrument met or exceeded operational specifications until it was removed from HST in December, 1993. However, the ability of HSP to carry out its primary program was nearly totally compromised by the poor performance of the telescope, i.e. the spherical aberration of the primary mirror which greatly amplified the affects of large spacecraft pointing jitter and "breathing". As a consequence, the real possibility of HSP opening a new era of astronomical photometry was lost. HSP data affected by various telescope problems as well as data in which these complications were relatively small, are shown. The excellent condition of the HSP after its return to earth is described.

1. INTRODUCTION

The Hubble Space Telescope afforded a unique opportunity to obtain photometry of unprecedented quality, not only in the ultraviolet but in the visible spectral region as well. The primary function of the HSP was extremely precise visual and ultraviolet photometry with high time-resolution. The small images expected, coupled with the absence of atmospheric scintillation noise and transparency effects, along with a stable pointing control system, allowed the use of much smaller apertures than is possible from the ground. In this paper we first describe the HSP as it was designed to take advantage of these expectations. After a brief description of the instrument in Section 2, various operational aspects are discussed including target acquisition, photometric modes of the HSP, and the disastrous effects on the instrument performance of the HST's primary mirror spherical aberration, "breathing", and pointing stability problems. Major internal instrumental calibrations are described in Section 4 and a discussion of the photometric performance of the HSP is presented in Section 5. Several illustrative examples of observations made by the HSP before it was replaced by COSTAR in the HST servicing mission of December, 1993 are given in Section 6. (COSTAR provided the remaining aft shroud instruments-two spectrographs and a camera-with images corrected for the aberrations produced by the HST primary mirror.) The paper concludes with a brief description of the condition of the instrument after its return to ground.

2. THE INSTRUMENT

2.1 Detectors and optics

The HSP was designed to be a very simple instrument with no moving parts. For wavelength coverage, functionality and redundancy, five detectors were used in the instrument. As shown in Figure 1, four of the detectors were image dissector tubes (IDTs) and one was a photomultiplier tube (PMT). The IDTs were ITT 4012RP Vidissectors. Two IDTs had CsTe photocathodes on MgF_2 faceplates (sensitive from 1200 to 3000 A) and are referred to as UV1 and UV2; two had bialkali cathodes on suprasil face plates (sensitive from 1600 to 7000A) and are denoted as VIS (used for photometry) and POL (used for polarimetry). Each IDT, its voltage divider network, and its deflection and focus coils were all contained in a double magnetic shield within the tube housing. The PMT was a Hamamatsu R666S with a GaAs photocathode. Quantum efficiency curves for these detectors are given in the HSP Instrument Handbook (Bless et al. 1992) available from the Space Telescope Science Institute (STScI).

Light from the telescope entered the HSP through one of four holes in the forward bulkhead of its enclosure. Three of these (for the photometry detectors, UV1, UV2, and VIS) were on an arc centered 8.1 arcminutes off-axis, while the fourth hole, for the POL detector, was about 4 arcminutes from the HST optical axis. After passing through the bulkhead hole, the light passed first through a filter and then through a focal plane aperture. In each of the three photometry channels, light was refocussed onto the IDT by an off-axis ellipsoidal mirror that converted the f/24 bundle from the telescope to f/15.6 at the detectors, with a corresponding change in scale from 3.58 arcsec/mm to 5.54 arcsec/mm. The POL detector was located directly behind its aperture plate and had no relay mirror that would otherwise complicate its use as a polarimeter.

The only unusual feature of the HSP's optical system was its filter-aperture assemblies, which were mounted behind each entrance hole in the forward bulkhead of the instrument enclosure (see Figure 2). Each plate for VIS, UV1 and UV2 contained thirteen filters mounted in two columns and positioned 36 mm ahead of the ST focal plane. At this location, the converging f/24 bundle of light from the ST was 1.5 mm in diameter, well within the 3 mm width of each filter. Each of the UV filters in the HSP was a multi-layer interference filter of Al and MgF_2 evaporated on fused quartz (suprasil) or crystal quartz for the near UV or on MgF_2 substrates for the far UV. The visual filters consisted of silver and cryolite layers deposited on clear glass, or were simple color glass filters. All of the substrates were 1/16 inch thick. In order to relate the three detectors photometrically, some duplication in the filters existed among the UV1, UV2, and VIS detectors. The full width at half maximum and the peak transmission of each filter are listed in Bless et al. 1992, where individual transmission curves can also be found.

For each of these filter plates there was an aperture plate containing 48 apertures located at the ST focal surface. Each of the filters had associated 1.0 and 0.4 arcsecond apertures, usually two of each. One of the filters was a clear window with twice the physical width of the others in order to accomodate the 10 arcsecond finding aperture together with several smaller apertures. In addition, the VIS detector had an aperture that passed light to a beamsplitting filter that reflected light to the PMT and transmitted a narrow band of near-UV light to the IDT.

Originally it had been expected that HSP would provide accurate photometry useful for various programs, including some in support of HST camera observations. With this in mind, filters were chosen which approximated standard bandpasses used by photometric systems in the visible and ultraviolet. As will become clear later in this paper, however, those expectations were never realized because the spherical aberration of the telescope's primary mirror made it impossible to achieve the requisite photometric accuracy. Consequently only a few filters were used for many of the observations.

The filter-aperture assembly for the POL detector differed considerably from those for the photometry detectors. It had four near-UV filters, one "above" the other, combined with four strips of 3M Polacoat analyzer each of which extended over all four filters, and which perpendicularly crossed the filters. The analyzers transmited radiation with E vectors at 45, 90, and 135 degrees with respect to the first analyzer. Associated with each of these 16 filter-Polacoat combinations was one 0.65 arcsec diameter aperture. A clear suprasil filter was positioned for use with the 6.0 arcsec finding aperture and with a pair of 0.65 arcsec apertures, all of which could be used for non-polarimeteric photometry, if desired.

Since the HSP had no moving parts, the telescope had to be pointed to allow radiation from the program object to pass through the desired filter-aperture combination and onto the photocathode. The resulting photoelectrons were magnetically focussed and deflected in the forward section of the IDT so that they passed through a 180 micron aperture and into the following 12-stage photomultiplier section. The 180 micron magnetically directed "read beam" corresponded to 1.0 arcsec on the sky for the photometry IDT's, and to 0.65 arcsec for the POL detector.

The time required for the spacecraft to slew between different filters on the same IDT was about 30 seconds, while that required to slew from one filter on one IDT to another on a different IDT was about twice that long. In an attempt to provide more nearly simultaneous photometry in two passbands, a beamsplitter was installed on each of the photometric IDTs. In this so-called "prism" mode, the read beam was moved back and forth between two filters. Its settling time was about 10 milliseconds so that observations separated by this interval (plus the sample time) could be made in two different passbands. The HSP was also capable of acquiring truly simultaneous two-color photometry using the VIS detector in conjunction with the PMT. These modes of operation will be discussed in more detail in Section 3.

2.2 Electronics

Each of the five detectors and its directly associated electronics was completely independent of the others. Each had a programmable high voltage power supply for the multiplier section of the detector, a preamp giving a voltage gain of about 7 that fed a pulse amplifier/discriminator, and a current-to-voltage converter for analog measurements (see Figure 3). Digital and analog signals from the detectors were sent to two 24-bit counters and an A/D converter, respectively, located in the detector controller. The latter received a sequence of parameters and instructions for its associated detector from the system controller that set up the particular observation and data collection desired. It also controlled the focus and deflection amplifiers on each of the image dissectors. The output of the pulse counters and A/D converter, along with the set-up parameters, were passed from the detector controller to the system controller.

The dual standby redundant system controller was made up of an Intel 8080 microprocessor, I/O ports, and memory. The latter consisted of 8K bytes of ROM for microprocessor programs, one 4K block of RAM for the 8080, four 4K blocks as a science data storage buffer, and a 4K block as a spare, which, if necessary, could replace any other 4K block. As its name implies, the system controller dealt with functions relevant to the instrument as a whole. For example, it decoded and distributed serial commands, programmed the detector controllers, acquired and formated both science and engineering data, and served as the interface with the HST command and data handling system.

Finally, a power converter and distribution system converted the spacecraft +28V DC power to the various outputs required by the HSP electronics and heater control system. This last was unusual in that it did not use thermostats to maintain pre-set temperatures, but instead operated under software control. That is, power to any of the heaters could be programmed on and off so as to keep the HSP at the desired temperature, as read by 29

thermistors; temperatures could be changed as conditions warranted. Such a thermal control system is extremely flexible and more reliable than one of conventional design (see Richards et al. 1993). The HSP remained within its temperature specifications throughout its orbital life.

Incidentally, in the Summer of 1993 a trend analysis of HSP temperatures since the instrument was in orbit indicated that the aft shroud sink temperatures were increasing by about 1^{o} C per year (see Richards et al. 1995). After this was called to their attention, the HST project verifed this result by a similar analysis of temperatures of the other Science Instruments. With the long lifetime of HST, this effect, caused by degradation of the thermal properties of aft shroud materials, is of obvious significance for the design of post-COSTAR HST instruments.

3. OPERATIONAL CONSIDERATIONS

3.1 Target acquisition

The HST provides three basic modes of target acquisition, referred to as interactive, onboard, and blind acquisitions. In the first two cases, the HST was pointed so that the program object fell in the finding aperture of the specified IDT. A 20 x 20 point raster scan covering the entire finding aperture was then made by the IDT to form a pseudo-image. In an interactive acquisition the image was displayed on a video monitor at the Observatory Support System at the STScI where an astronomer indicated the target with a cursor. Its position was then transmitted to the HST, which performed a small slew to acquire the star. During an onboard acquisition, the 20 x 20 step raster scan was sent to the onboard instrument computer that carried out a simple centroid calculation on the target and issued a small angle maneuver to center the target in the finding aperture. Because the image point spread function was much broader than expected, however, the accuracy of the simple nearest-neighbor centroid algorithm was somewhat degraded. We found that the centering was measurably improved if multiple acquisitions were performed in succession. Fortunately, the accuracy of the target acquisitions converged rapidly so that the centering was repeatable to within 0.05 arcseconds after only two consecutive acquisitions. This became standard procedure for observations beginning on June 5, 1991. After the star was centered in the finding aperture, another small angle manuever positioned the target in the desired aperture. The program object could be specified as the nth brightest in the field, where n could be up to 20; this option was never exercised, however, primarily because the telescope's spherical aberration made observing in crowded fields difficult. The default value of n was 1.

In the blind acquisition mode the target was placed directly in the desired aperture of the HSP. In practice, this was useful only for observations of the same target repeated within a short enough time period that the spacecraft roll angle had not changed significantly and the same guide stars could be used. The advantage of this mode was, of course, that valuable time was not spent acquiring the object (acquisition times, set by the observer, could take up to several minutes).

Observations of the Crab pulsar illustrate some of these points. In October of 1991 as part of the HSP Science Verification program, four 30 minute observations of the pulsar were made on successive days using a one arcsecond aperture, a broad visual filter (F400LP), and the fastest sample time of which HSP was capable, namely, 10.74 microseconds. In the first observation, the target was acquired interactively; in the following three observations, blind pointings were made because the same guide stars could be used. Data from the first, third, and fourth observations were within (sometimes barely) the photon statistics of their mean value; the corresponding count rate of observation 2, however, was 36 percent higher (about 5 times photon statistics) than the mean of the other observations. Data from the pointing control system indicated that for observations 1, 3, and 4, telescope pointings were within 0.05

arcseconds or less of each other, but the pointing for observation 2 differed by 0.22 arcseconds and apparently resulted in the pulsar being better centered in the aperture. The reader can find the individual pulsar light curves and a more extensive discussion of these points in Percival et al. 1993.

A combination of an on-board and a blind acquisition was also possible. In this case, an offset target was centered in the finding aperture using the on-board method described above. The telescope was then commanded to move by a pre-determined amount to place the target object in the finding aperture. This was followed by a small pointing maneuver that put the star in the desired aperture. Two fundamental requirements had to be met in order for a blind offset to be successful: 1) the distance between the two targets, the reference star and the program object, had to be small enough (generally less than 1.5 arcminutes) so that the same guide stars could be used in each case, and 2) the relative coordinates of the reference star and the program object had to be known accurately. Blind offsets were routinely used for acquiring stars for planetary occultations, because the presence of a nearby bright planet precluded the use of the normal on-board acquistion (see Elliot et al. 1993 and Bosh 1994).

A real-time interactive acquisition often could be avoided by acquiring an image of the field (using the Wide Field Camera, for example) and determining the program target's position well in advance of the observation. This technique is somewhat misleadingly called an "early" acquisition when in fact it simply uses HST to acquire a finding chart for the field. The subsequent acquisition would be either by the on-board mode or by combined on-board and blind modes, as described above.

3.2 Photometry modes

The HSP was designed to operate with the VIS, UV1 or UV2 detectors in any one of three modes: 1) single color photometry, 2) star-sky photometry, and 3) prism. In addition, the VIS and PMT detectors could be used together in the "split" or "occultation" mode.

In the star-sky mode, the read-beam was aligned with the star aperture and an integration performed; the read-beam was then moved to the sky aperture and another integration performed, after which the cycle was repeated. It was this operational mode that was the primary motivation for including, for each filter, two apertures of the same diameter separated by 30 arcseconds. In addition, the multiple apertures for each filter provided redundancy should an aperture be blocked by a speck of dust, for example.

With the same beam-switching technique, the prism mode was intended to obtain interleaved observations of the same object at two different passbands without changing telescope pointing. A beamsplitter/prism assembly allowed one to obtain photometric data in filter pairs centered at 2400A and 5510 A, 1350A and 2480 A, and at 1450A and 2620 A with VIS, UV1, and UV2, respectively. Because the IDT read-beam was switched back and forth between two filter/apertures in both the star-sky and prism modes, one must correct the observation times in the files provided by the STScI because these did not allow for the length of time required to move the read-beam between measurements. This time depends slightly on the data format; these times (accurate to about one microsecond) are specified in Table 1. Because of small misalignments in the beam splitter prisms, this mode was even more sensitive to telescope jitter than was the normal single color photometry mode. In addition, unexplained throughput losses of as much as factors of 5 to 10 in the beam splitter optics made this mode useful only for the brighter stars.

Finally, the HSP could also be used in what was referred to as the split or occultation mode. In this mode, truly simultaneous observations at 3200 A and 7500 A could be obtained. Light from the target passed through clear suprasil located on the VIS detector's filter plate, then through a 1.0 arcsecond aperture and onto a silver filter oriented at 45^{o} with respect to the incident beam. As described earlier, this beamsplitter transmitted blue light onto the relay

mirror that focused it onto the VIS IDT, and reflected the rest of the light to the PMT via a long pass red glass filter and a Fabry lens.

In any of these modes, the HSP could record data in both digital and analog format. The digital data format was a pulse counting mode that was useful for count rates < 10^6/sec (for a deadtime correction < 2%) because of the 40 nsec pulse counter deadtime. The pulse counting mode had a minimum integration time of 10.7 microseconds (more precisely, 11 pulses on a 1.024 megahertz clock). In the analog format the photocurrent was sampled for a gain-dependent time that was always less than 5 milliseconds. Because in the analog format the flux was sampled rather than integrated, the data have a considerably lower signal-to-noise compared to those obtained by pulse counting. The analog format had a time resolution of about 1 millisecond and was typically used for bright objects whose count rates exceed about 10^7 counts/sec, most often in target acquisition (which used the unfiltered finding aperture).

3.3 Length of exposures

The HST Science Data Formatter (SDF) protocol was designed with the imaging instruments in mind and was, therefore, somewhat cumbersome for the HSP. The SDF requires three set-up parameters: the number of words per line (WPL), lines per frame (LPF), and frames per observation (FPO). The selection of values for WPL and LPF is based on three factors: the image size, the fact that the image was integrated before the science data transfer was started, and finally that once begun, the transfer should proceed at a high rate. The SDF expects lines of data to follow each other within a strictly observed timeout period of 10 milliseconds. The FPO parameter represented successive frames so that the SDF allowed the HSP to insert an arbitrary amount of time between frames.

Because the HSP buffers usually were not large enough to store a whole "frame" (that is, a complete data collection) before initiating data transmission, data were sent to the SDF as soon as the first line of data (no more than 965 words) had been collected. Because of the 10 millisecond SDF timeout for each line, the HSP had to be prepared to transmit the next line of data within 10 milliseconds of the end of the previous one, which it could do only in the high speed (MHz) photometry regime. For slower sample rates, the HSP was forced to choose a LPF of unity, sending each line as a new frame. Finally, because the HSP firmware limited the frames per observation to 255, the maximum number of samples per science observation was 2 * WPL *FPO, or about 500,000 8-bit samples. This constrained the sample time for long observations. If the observation was lengthened, but the total number of samples was unchanged, then each sample had to be correspondingly longer. A detailed analysis can be found in White (1984). A modification to the HST ground system was installed in March, 1993 that removed this constraint allowing arbitrarily long data sets to be obtained.

3.4 Spherical aberration and pointing

Soon after the orbital deployment of the HST in April 1990, it was realized that the 2.4 meter primary mirror had -0.43 waves rms of spherical aberration at 6328 A (see Burrows et al. 1991 for details). The spherically aberrated mirror produces degraded images that are significantly poorer than those expected. The original specification of the HST stipulated that 70 percent of the energy would be concentrated within a 0.1 arcsecond radius at 6328 A. In actuality, the image consists of a sharply defined 0.1 arcsec radius core containing only about 15 percent of the energy, surrounded by a large and non-uniform halo more than 2 arcseconds in diameter. The non-uniformity results from diffraction by obscurations of the primary mirror pads and the secondary mirror supports. About 50 % of the light was lost at the 1 arcsec HSP photometry apertures and 75 % at the 0.65 arcsec polarimetery apertures. Because there were significant amounts of light beyond the edges of these apertures, any pointing error, drift or jitter resulted directly in photometric errors for data collected by the instrument (see below). In fact, the 0.4 arcsec apertures were unusable.

The Fine Guidance Sensors (FGS) of the HST have two modes of operation, coarse track and fine lock. Coarse track, a degraded mode in itself, is based on a centroiding algorithm that was intended for use when only faint guide stars were available or when the highest accuracy pointing was not needed. Fine lock, on the other hand, is based on an interferometric system that requires stars brighter than about V = 13.5. Originally, coarse track was designed to provide stable pointing to within 21 milliarcseconds for stars as faint as V = 14.5 and fine lock was intended to maintain stable pointing to within 7 milliarcseconds. For the first two years of operation, however, these specifications were not met during significant portions of orbital night. In particular, thermally-induced oscillations in the solar arrays during day-night transitions produced considerable pointing jitter for up to several minutes. Sometimes this jitter was of sufficient amplitude to cause the pointing control system to lose lock on one of the guide stars. In addition, random episodes of jitter occurred, attributed to "stiction" in the solar array spreaders (see Figure 4). Obviously, these effects degraded HSP photometry. Towards the end of 1992, however, adjustments to the pointing control feedback loops were completed so that the subsequent performance of the HST guidance system generally met the original fine lock jitter specifications.

Unfortunately, a few stability problems still affected HSP photometry. First, and least damaging, were residual solar array oscillations of the kind mentioned above that lasted for seconds rather than minutes. These events were reasonably isolated and distinctive and could be removed from data sets fairly easily. More damaging was the presence of pointing drift during and between observations. These effects are more difficult to calibrate or remove from HSP observations and can degrade the data significantly. They are detailed in Section 5 and can cause photometric errors of about 5% on various timescales. Furthermore, about one quarter of HSP observations made on coarse track were affected by an oscillation with a period of about 10 seconds, also probably caused by pointing instabilities (see Figure 5).

The sensitivity of HSP photometry to even small amplitide spacecraft jitter acting on the aberrated images was graphically illustrated by a test run in January, 1992. The purpose of the test was to establish the vibration environment that COSTAR would experience. Because the FGSs cannot measure jitter frequencies higher than about 25 Hz, and HST dynamic models were not considered reliable above 40-50 Hz, a jitter test was devised by the STScI using the HSP (see Bely et al. 1992). A star image was placed on the edge of an HSP aperture and the instrument sampled the light at 1000 Hz as various activities took place on the spacecraft. The low frequency body modes of the latter were of course easily detected, as well as the oscillation of the primary mirror on its support system at about 60 Hz. A small amplitude vibration caused apparently by the Goddard High Resolution Spectrograph's carousel motion was seen at about 94 Hz. Even more surprising, an oscillation was detected at about 300 Hz. It so happens that when the tape recorder is running at the 1 Mb rate, the teeth on the drive gear engage about 300 times/second. The mass of the ST is about 12.5 tons, yet the small tape recorder drive was producing an oscillation of about 1-2 milli-arcsec.

4. CALIBRATION

4.1 IDT calibration

The first step in the flight calibration of the HSP was to measure the position of the imaged HSP focal plane apertures in the IDT coordinate system. The aperture plate was illuminated with a flat field source, either the bright Earth or the Orion nebula, and imaged by rastering the IDT read beam over the photocathode. The resultant images were then analyzed to give the deflection coordinates for each aperture. The bright Earth was used for all of the UV aperture imaging because other flat field sources were too faint. However, it quickly became apparent that the Earth did not provide an adequate visible light flat field because clouds and

scattered light from the oceans gave rise to images with intensity spikes between 5 and 50 times the expected average brightness of the Earth. Consequently, the Orion nebula was used as a flat field source for the longer wavelength filters on the VIS detector. The deflection positions for each aperture were eventually established to within 50 milliarcseconds.

4.2 Relative aperture positions

After calibrating the IDT locations of the apertures, the next step was to calibrate the positions of the apertures in the HST focal plane. This was accomplished by measuring the photometric response through the selected aperture at each dwell point as the HST performed a scan in an s-shaped step-and-dwell pattern around an astrometric target star. An analysis of the time-varying signal, combined with a post-test determination of spacecraft pointing, yielded the focal plane locations of some selected apertures. The positions of the remaining apertures were established by modeling focal plane distortions with the known relative positions of the apertures. In this way, the position of each aperture in the focal plane was determined to within 20 milliarcseconds.

The calibration of the relative positions of the POL apertures was complicated by the somewhat poorer metrology of the POL aperture plate, which had drilled rather than photo-etched apertures. A special test was executed that measured the relative positions of all 16 polarimetric apertures with a bright star. The absolute positions of three apertures from the astrometric test (above) were combined with relative positions from the non-astrometric test to yield positions for all 16 apertures with a precision equal to that of the photometry apertures.

4.3 Calibration of the HST clock

We used observations of the Crab pulsar to calibrate the HST clock and to determine the uncertainty in UTC of a particular HSP event. Events on the HST are driven by a master 1.024 MHz oscillator. This same oscillator also drove the HSP microprocessor and data collection hardware. The HST Science Data Formatter kept a 32 bit software clock with a resolution of 125 msec. The HSP software clock was also a 32 bit counter, but its resolution was 1 msec. Assigning absolute times to the photometry samples collected by the HSP required establishing the zero point of the HSP clock with respect to the HST clock, as well as the zero point of the HST clock with respect to UTC.

The HSP/HST clock correlation was established by logging the HST clock value at the instant the HSP clock was set to zero. The HST/UTC correlation was established by time-tagging the receipt of certain telemetry signals at the time of their arrival at the White Sands ground station. A regression was then performed against the accumulated data to extract the coefficients of a quadratic polynomial mapping the HST clock onto UTC. The absolute time of an HST event was given by

$$T = T_o + (T_{v1} - T_{vo})r_o + (T_{v1} - T_{vo})^2 \, d_o/2,$$

where T_o is the absolute time corresponding to vehicle time T_{vo}; T_{v1} is the vehicle time of the desired event; r_o is the HST clock rate in seconds per count; and d_o is the HST clock drift rate in seconds per count squared. These coefficients are available from the Science Institute. With these two correlations we could convert any given HST or HSP time to absolute time.

We used these high precision correlations to compare various estimates of the absolute start time for a specific observation. The estimated starting time of an HSP observation could be obtained in a number of ways with varying degrees of accuracy. Calendar files, prepared long in advance of the actual observation, contained a crude estimate of the start time (typical accuracy was about three minutes), but included instrument setup time. The actual command load, in the form of a Science Mission Schedule (SMS), gave a refined estimate, with smaller overheads, but the estimates were given in "relative orbit time" and were subject to small changes as the HST orbit model was refined close to the epoch of the observation. The

uncertainty in these times was about 30 seconds. Finally, two post-observation estimates could be obtained: the time in the FITS header of the observer's data set, and the time derived from a special algorithm given in an Instrument Science Report (Percival 1992). Each of the post-observation methods uses the two correlations described above and both are accurate to within 10 milliseconds when using coefficients obtained near the time of the observation. The ISR algorithm was relevant if errors of a few milliseconds were important, as in planetary occultations, for example.

Observations of the Crab pulsar indicated that the accuracy of the ISR algorithm, when using the HST/UTC correlation closest to the epoch of the observation, could be within a few milliseconds of UTC. This accuracy was estimated by comparing the computed arrival time of the optical pulse with that of the radio pulse, taken from the radio ephemerides of Lyne and Pritchard (1992).

Additional information concerning the HSP and details of HSP data as received by the observer can be found in Bless et al. 1992 and in the High Speed Photometer section of the HST Data Handbook (Townsley et al. 1994), also available from the STScI.

5. PERFORMANCE

5.1 Short-term photometric stability

In August, 1991, we carried out a test designed to characterize the short-term photometric stability of the HSP/HST. The well-studied Ap star HD 60435, located in HST's "continuous viewing zone" (a small area of the sky surrounding each orbital pole in which an object is not occulted by the Earth), was continuously monitored for approximately five and a half hours with a sample time of 83 milliseconds. The data, rebinned to 100 point samples, are presented in the upper panel of Figure 6; their scientific anaysis is discussed elsewhere (Taylor et al. 1993). Two obvious effects are apparent in the data: 1) a sinusoidal oscillation with the period of the HST's orbit and 2) a slow linear increase in the count rate. Subsequent to the HD60435 observation, similar effects (same period, different amplitudes and linear slope) were seen in other HSP data. No plausible mechanism, either optical, thermal, power, or mechanical, could be found within the HSP that could produce these variations.

Soon after its discovery, it was suggested that this effect might be attributed to an incorrect application of the differential velocity aberration correction across the field of view of the telescope. In fact, it was eventually found that the HST flight software was indeed in error in that it applied the orbital velocity aberration correction about the optical axis of the telescope rather than about the off-axis location of the instrument aperture actually being used. Although this error accounted for some of the long term drift, a test with the aberration correction error removed still showed the effect.

In the meantime, however, this effect was seen also in data acquired by the other HST instruments. In fact it had been observed in WF/PC data (the so-called "breathing" effect) well before the HD 60435 observation, but its general significance had not been recognized. Breathing is the systematic variation in the image point spread function possibly caused by small temperature-induced changes in the position of the HST secondary mirror as the spacecraft orbits the earth. An empirical formula has been derived which represents the effect of breathing reasonably well (Hasan et al. 1993). According to this formula, the amplitude of the flux change is proportional to the difference between the instantaneous average of the temperatures measured at four points on the light shield directly in front of the secondary mirror, and their running average over the 96 minute HST orbit. Although this is suggestive and intuitively reasonable, it should be emphasized that this is not proof of a causal relationship between the light shield temperature and the breathing effect.

The Hasan model provides a plausible representation of the photometric variation observed by the HSP, but the model is not sufficiently precise, nor are its parameters always available, to allow a deterministic prediction and subsequent removal of the net effect.

We settled on subtracting a simple low-order fit to the data, whose terms represented the principal effects observed in photometry of standard stars that we attributed to breathing. These terms included a constant offset, a linear term (the "ramp"), and a sinusoidal function of the HST's orbital phase. The amplitude of the sinusoid is itself a linear function of time (we observed the amplitude of the sinusoid varying linearly in multi-orbit time series). Obviously, removing the breathing effect is made at the expense of eliminating any possible detection of intrinsic variability occuring near the HST orbital period. Also, one must be careful of any impact that removing these long-term trends might have on other parts of the frequency spectrum.

Figures 6, 7, and 8 show typical HSP data sets before and after the removal of the low-order breathing effects. Figure 6, discussed above, shows a 5.5 hour continuous observation of HD 60435, Figure 7 shows photometry of Cyg XR-1 over three orbits with earth occultations, and Figure 8 shows measurements of the stable star SAO 252703 taken over two HST orbits .

5.2 Detector Sensitivity

In order to monitor the response of all four IDT detectors (along with the transmission of their associated finding aperture windows, but not that of their filters), a test was devised that is relatively insensitive to the pointing problems and the orbital effects described above. In this test, a standard star was centered in the finding aperture where area scans (either 30 x 32 or 29 x 29 points) were made over the entire finding aperture so that all of the stellar flux was measured, regardless of any small image motions or miscenterings. This technique produces the most reliable photometry obtainable with HSP over a long time period. These observations were made three times each in 1991 and 1993, using the star VID 998, spectral type F5. Unfortunately, this series ended in June of 1993; to extend the measurements to the end of 1993, data taken in a similar manner using the HST standard star BD $+75^{o}325$, spectral type O5p (Bohlin et al. 1990) were normalized to the earlier data, after which all of the observations of a given detector were normalized to the first measurement of the series. The photon noise is given for each data set.

The results for the UV1, UV2, and POL detectors (with additional data for the latter as described below) are given in Figures 9a, 9b, and 9c, respectively. Both UV detectors were stable, indicating that neither their crystal quartz finding apertures nor their MgF_2 tube windows nor their cathode materials degraded in any significant way over the orbital life of the HSP. Similarly, the response of the POL detector (suprasil clear aperture and MgF_2 window) remained constant. Incidentally, operational detector temperatures varied by no more than a few degrees and had no effect on photometric performance.

In marked contrast, the sensitivity of the VIS detector declined steadily until the latter part of 1993 (Figure 9d). In order to have as complete temporal coverage of this decline as possible, area scans made in 1992 of BD $+75^{o}325$ with the VIS and POL detectors at lower spatial resolution (20 x 20 points), presumably yielding data of somewhat poorer precision, were used. (Recall that the POL and VIS detectors are identical, differing only in their associated filters, so that their behavior should be similar.)

Because the VIS data were not constant, the normalizing factor derived from the POL data had to be used to combine the observations of the two stars. This leads to an uncertain, but most likely small, error in the derived detector sensitivity in 1992 and after June 16, 1993 (the data for which were obtained using the star BD+$75^{o}325$). The qualitative result is certainly not obscured, however: after a steady decline in sensitivity, a recovery occurred sometime between 28 August and 02 November, 1993. No such behavior is seen in the POL detector data.

Since the transmission of the POL detector's finding aperture and tube window (both suprasil) did not change during this time, it would appear reasonable to assume that the corresponding elements of the VIS detector did not change either. This suggests that the problem is in the detector itself or its electronics. The latter operated normally leaving only the detector suspect, but apart from its sensitivity, its performance appears to be as expected. At the present time no plausible explanation of the behavior of this detector is known.

5.3 Absolute Flux Calibration

The absolute calibration of HSP photometry was always intended to be determined only after launch, using standard stars. The best that could be done before launch was to combine separate measurements of detector quantum efficiency, mirror reflectivities, and filter bandpasses to give an estimate of the overall HSP performance. Even under favorable circumstances this method gives only moderately reliable results. The various HSP component calibrations, however, were made from six to ten years before launch so that their relevance to post-launch conditions is dubious at best. We give here only the results of absolute flux calibration tests using a standard star.

The primary HST flux standard BD+75°325 (O5p, Bohlin et al. 1990) was observed seven times in the 21 months between March, 1992 and December, 1993. In contrast to the detector sensitivity test just described, this test was designed to measure the overall response of the HSP in several filter bandpasses. With the telescope's spherical aberration, this was not a clean test, obviously, because the throughput of the one arcsec photometry apertures associated with the various filters exhibited errors caused by the orbital effect and pointing errors.

Some results of these observations for the UV1 and UV2 detectors are summarized in Figure 10. The Figure gives the logarithm of observed count rates from BD+75°325 through various filters, each normalized to the first observation of the series. The first 4 measurements were made between 3 March and 16 October, 1992, while the last 3 were taken between 28 August and 3 December, 1993. No systematic decline in count rate is seen over the seven month span of the 1992 data, nor over the three month period of the 1993 measurements. The most striking feature of the data is that the last observation of 1992 is always higher than the preceding measurement and often is the highest of the year. It so happens that the telescope was refocussed just after the third set of observations (August 23), producing a somewhat smaller image and so an increased flux through the one arcsecond apertures. Perhaps this effect is seen in these data, though demonstrating it quantitatively is difficult.

Apart from this effect, the data do not lend themselves to easy generalizations. The 1993 measurements, which began 10 months after the end of the 1992 set, are often, but not always, a few percent lower than the latter data. This is particularly striking in the F145U2 filter. If this effect is real, it might have been a consequence of systematically poorer telescope pointing during this period when one of the Fine Guidance Sensors had problems and was turned off. Alternatively, it might indicate a slow decrease in the transmission of the MgF_2 substrate of that filter. This effect, however, is not seen in the F135U1 filter which also has a magnesium fluoride substrate. All the other filter substrates in Figure 10 are suprasil, except for F278U2 which is a Schott glass. Furthermore, the 1993 detector U1 observations show a rising trend. It appears likely that if the filters suffered any radiation damage, this has been masked by other, larger effects.

These data demonstrate that the random error in absolute photometry with the HSP is roughly ±5 %. This error is primarily attributed to breathing effects and to small differences in telescope pointings from one observing run to the next, with corresponding changes in aperture throughputs. (Recall that the detector sensitivity is stable to better than 1 %.) Thus,

photometric accuracy no better than about 5 % is the best that can be expected between observations of the same object taken at different times.

5.4 Linearity

In addition to characterizing the short-term photometric stability of the HSP, we also carried out tests to determine the linearity of the response of the HSP. We measured six photometric standard stars through the 551W filter on the VIS detector that range in brightness from V = 5.11 to V = 12.79 (an observation of a 15th magnitude star was too short to give a reliable measurement). The HSP instrumental magnitudes were transformed to the V system by compensating for the orbital effect and then fitting the resulting data, including a color term, to the V magnitude system. Table 2 shows that treated in this way, the data indicate that the response of the HSP is linear to within 0.01 mag. over this range of magnitudes. This result strongly suggests that "correcting" HSP data for breathing in this manner (and for similar purposes) is legitimate.

5.5 Polarimetry

As mentioned earlier, one IDT was dedicated to broadband measurements of linear polarization in the UV. The wavelength ranges of the four bandpasses available for polarimetry are given in Bless et al. 1992. Cut sheets of 3M "Polacoat" were placed in the bandpass-filter assembly to act as analyzers. Four different analyzer orientations were used with each filter, denoted as 0^o, 45^o, 90^o, and 135^o from the orientation of the E vector of the transmitted radiation relative to the 0^o analyzer. The normalized Stokes parameters were then derived from photometric measurements through pairs of apertures: $q = (I_0 - I_{90})/(I_0 + I_{90})$ and $u = (I_{135} - I_{45})/(I_{135} + I_{45})$.

The Stokes parameter u is the negative of that usually defined because the nomenclature adopted for the filters has their orientation increasing clockwise when viewing the sky through them. Because of small intrinsic variations in the sensitivity of the IDT photocathode at different locations, the relative throughput for constant intensity unpolarized light of each aperture in a set of four had to be taken into account before polarimetric measurements could be made.

HD115271 (A7V) and HD176425 (A0V), both of which exhibit no significant polarization ($p < 0.02\%$) in the U and B bands, were verified as also having no significant polarization in the UV by using each individual aperture on the POL tube as a single channel polarimeter. The entire HST was rolled to $+60^o$ and -60^o relative to its normal orientation and photometric measurements were taken of both stars at each orientation. The linear polarization (and its position angle) in the stellar radiation can be derived from the photometric measurements at these three angles (Ohman 1949). Because a single aperture was used at all three orientations, the relative throughput of different apertures was not required in order to measure the polarization. HD115271 and HD176425 were both found to be unpolarized ($p < 0.2\%$) in the UV. These two stars were then observed in the normal observing mode to measure the correction factors for each aperture in all four bandpasses. These correction factors by which one divides the measured count rate to normalize every aperture in that bandpass to the same throughput for unpolarized light are given in Table 3.

Measurements of the Stokes parameters obtained in the internal coordinate system of the polarimeter are referred to the orientation of the E vector transmitted by the 0^o analyzer. Conversion to the equatorial coordinate system is possible given the roll angle of the telescope. The position angle of the 0^o analyzer in the equatorial coordinate system is the parameter "PA_APER" in the header accompanying each data set. The position angle of the polarization in equatorial coordinates is the sum of this position angle and the position angle of the polarization measured in the internal coordinate system of the polarimeter. This conversion angle was verified on orbit by observing stars with known position angles of polarization in the visible.

The photometric uncertainty in the observations of the calibration stars produces the principal uncertainty in the values of the normalization factors. Based on the observations of the individual calibration stars, the uncertainty on the normalization factors contributes an uncertainty of ±0.2% to the derived Stokes parameters in the F327M and F277M bandpasses, and ±0.4% in the F237 and F216M bandpasses. These uncertainties are systematic, in that they refer only to the accuracy of the measurement, not its precision. The precision (relative uncertainty) of any two measurements was found by repeated measurements of bright stars over a duration short compared to the timescale of any known photometric or polarimetric variability in them. The deviations from the mean of the measured values of q, u and p are consistent with a normal distribution with standard deviation ±0.3% in both the F327M and F277M bandpasses. Any uncertainties resulting from the photon statistics of the photometric measurements add in quadrature to this polarimetric uncertainty.

Because the polarization is derived from photometric measurements, any process that lowers photometric precision will also lower polarimetric precision. One such effect is breathing which is most likely always present, but with a variable amplitude; another is the re-acquisition of guide stars on the orbit following an occultation of the target by the Earth. Observations with the POL detector were made with 0.65 arcsec apertures, increasing both effects as compared with their consequences when one arcsec apertures are used. For example, the small but unavoidable variation in the pointing direction of the HST from orbit to orbit (a few milliarsec even with the double acquisitions) resulted in a photometric variability of 1-2% in the count rate of a constant intensity source from orbit to orbit because a slightly different part of the image passes through the aperture. Polarimetric measurements in all four orientation analyzers (or at least, the pair involved in a single Stokes parameter measurement) had to be completed within the same orbit to attain a polarimetric precision better than 1-2%. Multiple measurements of the Stokes parameters of a non-varying object from different orbits, each individual measurement completed within one orbit, can then be added together to improve the statistical precision on faint targets.

An example of the performance of this simple polarimeter is given by observations of the OVV quasar, 3C345 (V = 17). The total integration time in all four analyzer orientations, along with corresponding background measurements, was 64 minutes in the 2160 A bandpass and 48 minutes in the 2770 A band. The data were obtained over several orbits, separated by occultations of 3C345 by the Earth. Though these observations were made using double acquisitions, they were still somewhat affected by the reacquisition effects mentioned above. At 2160 A, the measured polarization is 11.0 $\pm$ 4.2%, with a position angle of 61 $\pm$ 11^{o}; at 2770 A the corresponding values are 6.8 $\pm$ 2.4% and 60 $\pm$ 10^{o}, respectively (see Dolan et al. 1994 for details).

5.6 Problem with fast times series

A significant problem of as yet unknown origin can occur in time series data sets. On two different occasions, autocorrelation analyses revealed an unexpected spike of power at lags of 8.6 ms and 9.4 ms. These features were caused by small patches of time series data being copied from one part of the data set to another.

The data are organized in packets inside the HSP, and are treated as packets all the way through the system until the HST Ground System at the STScI reformats them into a simple time series. We discovered that data from the beginning of packet 7 were appearing at the beginning of packet 8, and similarly for packet pairs 15 and 16, 23 and 24, and so on. The packet collection times in these two isolated instances were 8.6 ms and 9.4 ms, accounting for the results in the autocorrelation. The length of the duplicated stretch varied randomly from 12 to 24 samples.

Extensive analyses were performed by the HSP team and by experts in the operation of the SDF, the packet interface to which the HSP sent data. No likely suspects were found. A simple "numerological" analysis also failed to implicate any specific subsystem. For example, the HSP maintains 8 internal packet buffers, easily leading one to suspect a connection with the period-of-8 repetition described above. However, it is difficult to imagine a buffer usage error affecting pairs of packets. That is, packets 0 and 8 share buffers, not 7 and 8. On the other hand, packets appear pairwise in the SDF, which maintains two ping-pong packet buffers. The SDF can generate defective packet time stamps, which then cause the ground system to put packets in the wrong order, although this is not expected to change the contents of a packet.

This autocorrelation test was performed on many data sets taken with precisely the same instrument configuration, with no irregularities found. Only four data collections (taken on two days less than a week apart) have been discovered that show this effect. In any case, users who took data at sample rates exceeding 1 KHz are encouraged to do an autocorrelation and look for spurious power at lags equal to a packet collection time, which is the sample time multiplied by the number of samples per packet. The latter value is given in the SMS command load or more conveniently, in the FITS headers for the data.

6. EXAMPLES OF PHOTOMETRY

The HSP was the science instrument most severely affected by the greatly degraded performance of the pre-COSTAR HST. The HSP's photometric accuracy and repeatability were severely compromised not only by the primary mirror's spherical aberration, but also by spacecraft jitter, breathing, and loss of lock effects that often mimicked properties of astronomical objects in both amplitude and frequency. As a consequence, most of the primary goals of HSP-for example, detection of 5 minute oscillations in solar-type stars, measurement of micro-oscillations in luminous stars and in the nuclei of active galaxies, direct detection of the cooling of a white dwarf-could not even be attempted, much less reached. The expected improvement in photometry with HST comparable to that achieved in imaging turned out to be impossible.

The photometer could still carry out programs in some photometric regimes, however. Not surprisingly, these regimes differed in some way from those affected by the HST: very high time resolution, aperiodic events, low count rates, and non-sinusoidal variability. Figure 11 illustrates some of these points. The top panel shows the Crab pulsar in the ultraviolet at an effective time resolution of 20 microseconds (Percival et al. 1993). The main peak was resolved in time, and was matched in absolute time to the radio peak to within about 1 millisecond.

The second panel shows a typical light curve of the eclipsing dwarf nova Z Chamaeleontis at 1350 A, rebinned from 1 second per sample to 10 seconds per sample (Robinson, E. L. et al. 1995). Even in the raw data events of significant interest are visible. The eclipse minimum happens in two steps; the white dwarf is first occulted, followed by the occultation of the hot spot at the edge of the accretion disk. The sharp egress marks the reappearance of the white dwarf.

The third panel of Figure 11 shows a flare from the dMe flare star CN Leo (Gl406) through a narrow band filter at 2400 A rebinned from 9.8 milliseconds per sample to 0.98 seconds per sample (Robinson, R. D. et al. 1995). Again, even in the raw data the size of the event, the presence of microstructure, and the expected exponential decay are immediately apparent. In this Guest Observer program one large flare, shown in the figure, two smaller flares, and 29 microflares were detected in four 30-minute observations.

Data from one segment of a stellar occultation by Saturn's rings are shown in Figure 12. (Elliot et al. 1993). These data have been rebinned from 0.15 seconds per sample to 1.5

seconds per sample. The background light (from Saturn's rings) has not been removed; the changing background produces the overall rise in signal of the data segment. The shallow, flat-bottomed dips in the data correspond to occulations of the star by features in Saturn's optically thin C ring. Times of these occultations are measured and included in a geometric model for the event, producing information about the orientation and precession of Saturn's pole, as well as the kinematics of these and other ring features (Bosh 1994).

7. THE STATE OF HSP ON ITS RETURN TO EARTH

The most important consideration in planning the post-mission activities was to preserve information. Activities were scheduled to minimize the chance that a particular inspection, test, or operation would destroy information that might be retrieved by a later activity. The primary objectives in post-mission activities were: to support GSFC requests for information (for example, system level contamination investigations); to determine if there might be additional information about the puzzling behavior of IDT 3 during the mission; to determine if problems or failures at the subsystem or component level were undetected at the system level; to compare the post-mission performance of the HSP with similar tests conducted before integration into HST; to assess the condition of the HSP for possible reflight; and to learn whatever might be usefully applied to future instruments by determining how various construction techniques, parts, materials, or processes withstood the rigors of integration, system test, flight, and return to earth.

The shuttle returned to Kennedy Space Center with the HSP inside the SIPE (Scientific Instrument Protective Enclosure) into which it had been placed during the December, 1993 servicing mission. The HSP remained in this enclosure while it was transported to GSFC, arriving there in January, 1994.

In late January, the HSP was removed from the SIPE at GSFC and its exterior carefully inspected. No evidence of gross contamination or damage to the HSP was found. Contamination samples were taken and analyzed. The overall contamination found on the HSP was equal to (or in some cases less) than the level found before spacecraft integration (see Hughes 1994). Before proceeding further, a complete set of HSP interface and functional tests, including a very crude throughput check, was performed. All HSP functions were verified and no malfunctions or anomalies occurred. These tests included, for the first time since launch, a complete verification of all the HSP redundant electronics, none of which was powered during the mission.

Exterior panels were removed to allow the ODS to be inspected. Again, everything appeared to be as it was before launch. The HSP latch fitting interfaces were tested for stress corrosion cracks in the same manner as before launch, using both eddy current and ultrasonic flaw detection tests (Lugmayer 1994). No anomalies were detected by either method, indicating that there were no adverse consequences from the use of 2024 aluminum. (After it was already incorporated in the HSP, 2024 aluminum was not recommended for use by Goddard.) The filters showed no significant changes from their pre-launch appearance. In mid-July the HSP was shipped to UW Madison where tests were delayed for six months as a result of the failure of a freight elevator the day the instrument arrived.

At the HST Returned Hardware Seminar held at GSFC in December 1994, particular interest was expressed in determining the source of contamination observed on the WFPC optics. As a consequence, additional samples were taken and analyzed at Lockheed and Goddard. No material corresponding to that found on WFPC was detected. About a year after the seminar, an independent study of the effects of the space environment on optical surfaces was initiated at Ball Aerospace (see Fleming 1996). In this work the reflectance and scattering properties of one of the HSP off-axis ellipsoid mirrors were measured. These indicate that after three years

in orbit the reflectivity from about 5000 to 2500 A compared to the pre-launch values had decreased by about one percent. After the mirror was washed, however, the reflectance from 4000 to 2500 A increased by about 2 percent, suggesting that a certain amount of contamination had taken place soon after the mirror was coated, but before its reflectance was measured in 1982. Analysis of surface residue indicated that the substances found could all be considered handling contaminants. In summary, after 8 years on the ground and 3 years in orbit the mirror, and presumably the HSP in general, remained quite clean.

A series of electrical and functional tests of the entire instrument including a complete long form functional test was performed and all functions, including those using redundant units that had not been operated during the mission, operated without any failures or anomalies.

The HSP hardware was built in the late 1970s and early 1980s with integration of the flight HSP beginning in 1981. The original ST program requirements specified that all hardware shall be desigined for a service life of two and one-half years in orbit plus three years ground test time with an operating duty cycle of 50 percent in orbit, 20 percent on the ground. So after about 15 years, over three and a half of which were in orbit, it was interesting to test the HSP subsystems to see how their characteristics might have changed over that time. Also, since flight spare boxes were manufactured at the same time as the flight units but kept in storage on the ground, it was possible to determine if there were any effects due to spacecraft integration, test, and flight.

Four high voltage power supplies, two flight units and two spares, were inspected and subjected to functional tests at -40^{o} C, 0^{o} C, +24^{o} C, and +40^{o} C. The results were compared to similar data taken in April 1987. All units functioned well within specification and differences in the March 1995 and April 1987 data were within the measurement error, for example, a few hundredths of a percent in output voltages. Visual inspections revealed no changes in the flight or spare units and it was concluded that these units are very stable and even could be reflown as is.

The flight spare PCDS (Power Conditioning and Distribution Subsystem) was also tested and its performance was indistinguishable from that of the original acceptance tests.

The major unsolved mystery of the HSP is the change in the sensitivity of the VIS detector (IDT #3) described earlier. A series of tests was run in March 1995 to explore this anomaly. First the VIS detector was operated for about a week exposed to a constant (but uncalibrated) light source. It operated at expected noise levels and with a reasonable response to the light source. Next a two detector data collection was run for about a week to compare the response of the POL and VIS detectors. The two detectors behaved similarly; in particular, there was no evidence of instability or change of throughput in the VIS detector relative to the POL detector during the test. Next the high voltage power supplies (HVPS) for both the VIS and POL detectors were removed for box level testing and replaced by flight spares which had just been tested (and found to perform just as they had years earlier). The two detector test was repeated with results identical to the first such test, indicating no HVPS dependency on the performance of the VIS tube. Finally the two detector test was run with the VIS detector replaced by the flight spare. Again, no significant difference in performance could be seen. The orbital behavior of the VIS tube remains a mystery.

ACKNOWLEDGEMENTS

In a program of the size and longevity of HST, it is impossible to mention by name all of the talented and dedicated engineers, technicians, scientists and students at the Space Astronomy Laboratory and the Space Science and Engineering Center, both at the University of Wisconsin-Madison, at the STScI and the many NASA facilities and commercial organizations who contributed to the design, construction, testing and operation of the HSP. We are grateful to

them all. It is appropriate to mention two individuals, however, not only for their own major contributions to the HST program, but also as representatives of the commercial firm responsible for integration of HST and of the NASA center with the overall responsibility for the program: Dr. Domenic Tenerelli of Lockheed and Mr. Jean Olivier of the Marshall Space Flight Center. Their dedication and efforts were of inestimable value to this project.

BIBLIOGRAPHY

Bely, P., Lupie, O., Hershey, J., and Walter, L. 1992, SESD-92-15, Space Telescope Science Institute.

Bless, R. C., Percival, J. W., Walter, L. E., and White, R. L. 1992, HSP Instrument Handbook, Space Telescope Science Institute.

Bohlin, R. C., Holm, A. V., Harris, A. W., and Gry, C. 1990, ApJS, 73, 413.

Bosh, A. S., 1994, Ph.D. thesis, Massachusetts Institute of Technology

Burrows, C. J., Holtzman, J. A., Faber, S. M., Bely, P. Y., Hasan, H., Lynds, C. R., and Schroeder, D. J. 1991, ApJ, 369, 21L.

Dolan, J. F., Boyd, P. T., Wolinski, K. G., Smith, P. S., Impey, C. D., Bless, R. C., Nelson, M. J., Percival, J. W., Taylor M., Elliot, J. L., Robinson, E. L., and van Citters, G. W. 1994, ApJ, 432, 560.

Elliot, J. L., Bosh, A. S., Cooke, M. L., Bless, R. C., Nelson, M. J., Percival, J. W., Taylor, M., Dolan, J. F., Robinson, E. L., and van Citters, G. W. 1993, AJ, 106, 2544.

Hasan, H. and Bely, P. 1993, BAAS 183, #113.06

Hughes, D. 1994, HST FSM Contamination Report, P442-0667 1994

Lugmayer, J. C. 1994, Report No. LAJ-1850-94

Lyne, A. G. and Pritchard, R. S. 1992, Jodrell Bank Crab Pulsar Timing Results, Monthly Ephemeris, University of Manchester.

Ohman, Y. 1949, *Polarization Measurements in Astronomy*, High Altitude Obs., Boulder, Colorado)

Percival, J. W. 1992, HSP Instrument Science Report #12, Space Telescope Science Institute.

Percival, J. W., Biggs. J. D., Dolan, J. F., Robinson, E. L., Taylor, M., Bless, R. C., Elliot, J. L., Nelson, M. J., Ramseyer, T. F., van Citters, G. W., and Zhang, E., 1993, ApJ, 407, 276.

Richards, E. E., Percival, J. W., Sitzman, J., and Jones, T., 1993. SPIE, 1945, 224.

Richards, E. E., Townsley, L., and Wiggins, C. 1995, SPIE, 2478, 130.

Robinson, E. L., Wood, J. H., Bless, R. C., Clemens, J. C., Dolan, J. F., Elliot, J. L., Nelson, M. J., Percival, J. W., Taylor, M., van Citters, G. W., and Zhang, E. 1995, ApJ, 443, 295.

Robinson, R. D., Carpenter, K. G., Percival, J. W., and Bookbinder, J. A. 1995, ApJ, 451, 795.

Taylor, M., Nelson, M. J., Bless, R. C., Dolan, J. F., Elliot, J. L., Percival, J. W., Robinson, E. L., and van Citters, G. W. 1993, ApJ, 413 125L.

Townsley, L. C. 1994, in HST Data Handbook, Space Telescope Science Institute, ed. Stefi Baum.

White, R. L. 1984, HSP Instrument Science Report #1, Space Telescope Science Institute.

FIGURES

Figure 1. Schematic layout of the optical components of HSP.

Figure 2. The filter/aperture assembly used with each image dissector detector. The prism mode beam-splitters are not shown.

Figure 3. A block diagram of the HSP electronics.

Figure 4. A short section of data obtained during the short-term photometric stability test of the HSP. The top panel shows the photometric signal in counts/bin as a function of time. The large excursions result from solar array induced pointing instabilities as the HST crosses the day-night boundary. These variations occur with a frequency of about 1 Hz and typically last for about 10 -15 seconds. The middle panel results from transforming the photometric signal to a position error (in arcseconds) using a transfer function measured for HSP one arcsecond apertures with the Mission Support Calibration fine alignment test. As can be seen, excursions of this type can be as large as nearly one arcsecond. The bottom panel is the first derivative of the position error data with respect to time, which indicates the angular speed of the telescope during the event. Velocities are seen to range up to 2 arcseconds per second.

Figure 5. Plots similar to those shown in Figure 4 for a star that was observed as part of the color transformation test of the HSP. These data represent the full data collection through a single filter and are representative of most of the data collected for this test on that particular day. These data are uniformly contaminated by slow 0.1 Hz oscillations that correspond to a peak-to-peak pointing excursion amplitude of about 0.1 arcseconds. This particular pointing error seems to be associated with the coarse track pointing mode and is present in about 25% of HSP data taken in that mode.

Figure 6. The upper panel shows a 5.5 hour observation of HD 60435 made with a UV1 broad-band filter (peak transmission at 2400 A, 550 A FWHM) rebinned to 8.24 second time resolution. The dominant variations in these data are a smooth sinusoidal oscillation at the HST orbital period and a linear increase in count rate from cycle to cycle. These variations are not exclusive to HSP data and are related to changes in the telescope as the HST orbits earth. The V2 and V3 positions of the FGSs also are shown (+) in this figure, but neither exhibits variations characteristic of those seen in the photometry. The solid line superimposed on the photometric data is the least squares low order fit that models the orbital variations. The lower panel shows the residuals of the modeled data with dashed horizontal lines that represent the expected one sigma error based on photon statistics, namely, N. The short time scale fluctuations seen in both plots are caused by intrinsic variability of HD 60435.

Figure 7. Plots similar to those shown in Figure 6 for the X-ray binary Cyg XR-1. The upper diagram shows three 30-minute observations obtained over three consecutive orbits of the HST using the clear aperture on UV2. In addition, the corresponding V2 and V3 positions of the FGSs are shown (+). In contrast to the data in Figure 6, variations in the FGS data obtained during this observation, especially in the V2 coordinate, are seen to occur on time scales similar to those detected in the photometry. The residuals of the modeled data are shown in the lower panel where the dashed horizontal lines denote the expected fluctuations (one sigma) based on photon statistics.

Figure 8. Counts/second as a function of time for the constant photometric source SAO 252703. These data also exhibit a dominant sinusoidal oscillation at the HST orbital period as well as a linear change in count rate. Notice, however, that in this data collection (and in contrast to those in Figures 6 and 7), the amplitude of the sinusoid has a time-dependent component. This model is shown as a solid line in the top plot and the residuals of the modeled data are shown below.

Figure 9. The flux, normalized to the first measurement of each series, as a function of time for observations of the star VID (Van Altena ID) 998 and BD+75^{o}325 made through the finding

apertures on each of the HSP detectors. Photon noise is no greater than the size of the data points. The count rates with UV1, UV2, and POL remained essentially constant over the HST orbital lifetime, while the VIS detector showed a significant reduction in sensitivity followed by a recovery towards the end of 1993.

Figure 10. Relative throughput observations made between March, 1992 and December, 1993 using various filters on detectors UV1 and UV2. Each set of observations is normalized to the first measurement of the series.

Figure 11. The top panel shows broadband ultraviolet observations of the Crab pulsar at 20 microsecond resolution. In the middle panel 45 minutes of photometry are given of the cataclysmic variable, Z Cha at 1550 A, during quiescence. The one second samples have been binned to 10 seconds. Even with the small count rate and the resulting large photon noise, one can see the occultation of the white dwarf by the main sequence secondary (the first drop in the eclipse), as well as the drop resulting from the occultation of the bright spot on the accretion disk surrounding the white dwarf. The bottom panel displays 2400 A photometry of a flare on CN Leo. The data are binned to 0.98 seconds per sample.

Figure 12. One segment of a stellar occultation of Saturn's rings showing several ring features.

TABLES

Table 1: Time required to move an IDT read beam in various data formats
Table 2: Linearity of HSP over 7 magnitudes
Table 3: Polarization normalization factors

Table 1

Data Format	Time (msec)
1=1-byte	19.60
2=2-byte digital	19.63
3=3-byte digital	19.65
4=2-byte analog	19.82
7=3-byte digital+2-byte analog	19.68

Table 2

known mv	measured mv
5.111	5.113
7.184	7.184
7.247	7.247
8.060	8.057
9.570	9.571
12.790	12.790

Table 3

Filter	P0°	P45°	P90°	P135°
F327M	1.0269	0.9591	0.9851	1.0290
F277M	1.0302	0.9274	1.0020	1.0403
F237M	1.0075	1.0022	0.9995	0.9907
F216M	0.9766	0.9774	1.0332	1.0128

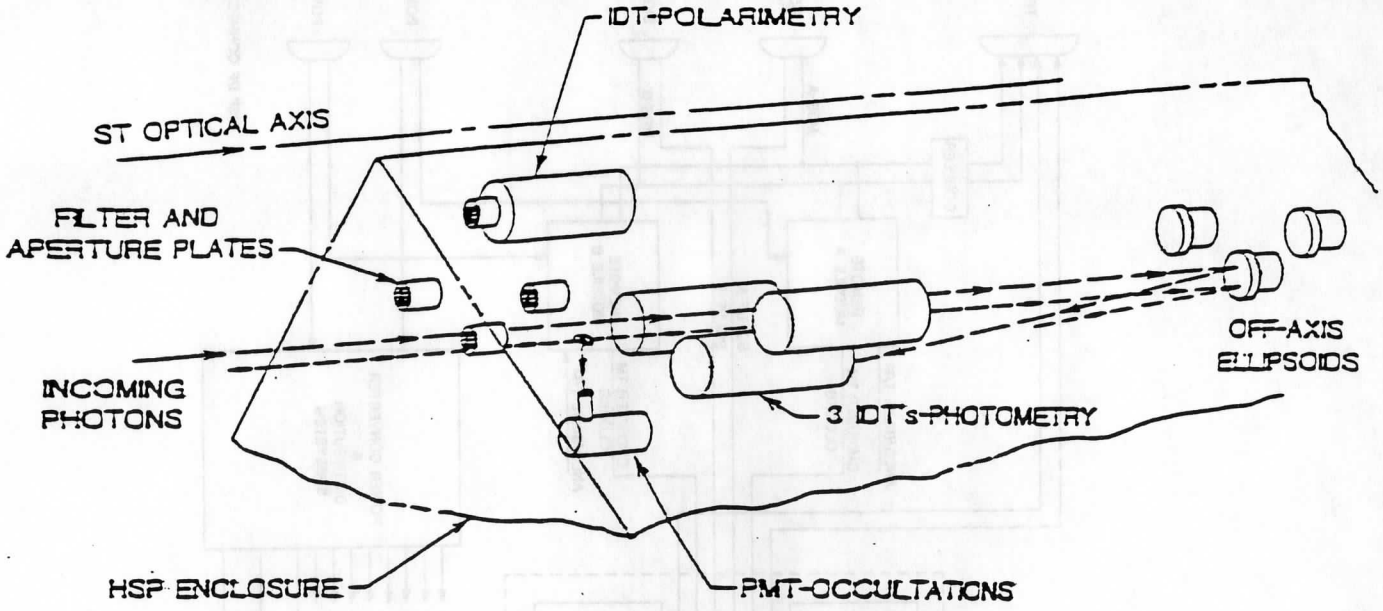

HSP DETECTOR ARRANGEMENT

Figure 1

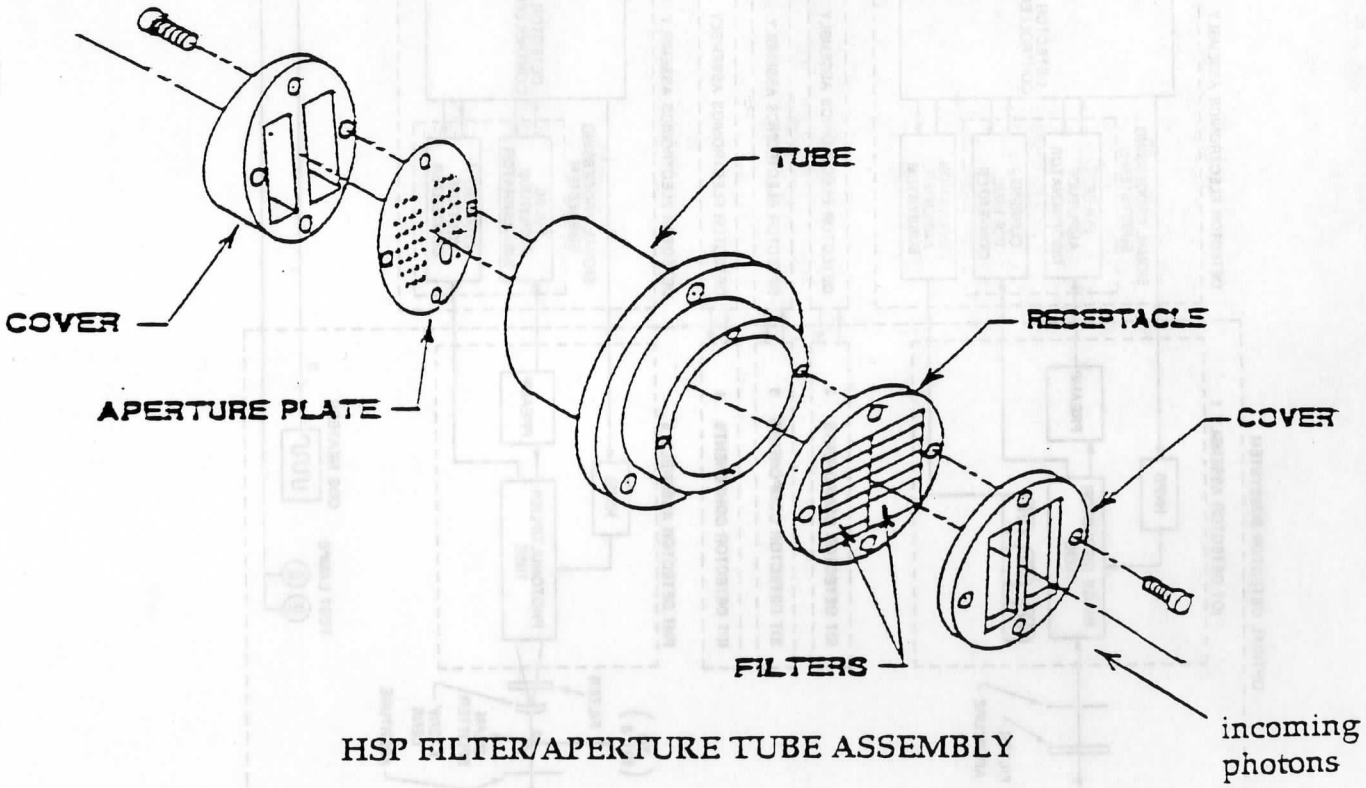

HSP FILTER/APERTURE TUBE ASSEMBLY

Figure 2

HSP SYSTEM BLOCK DIAGRAM

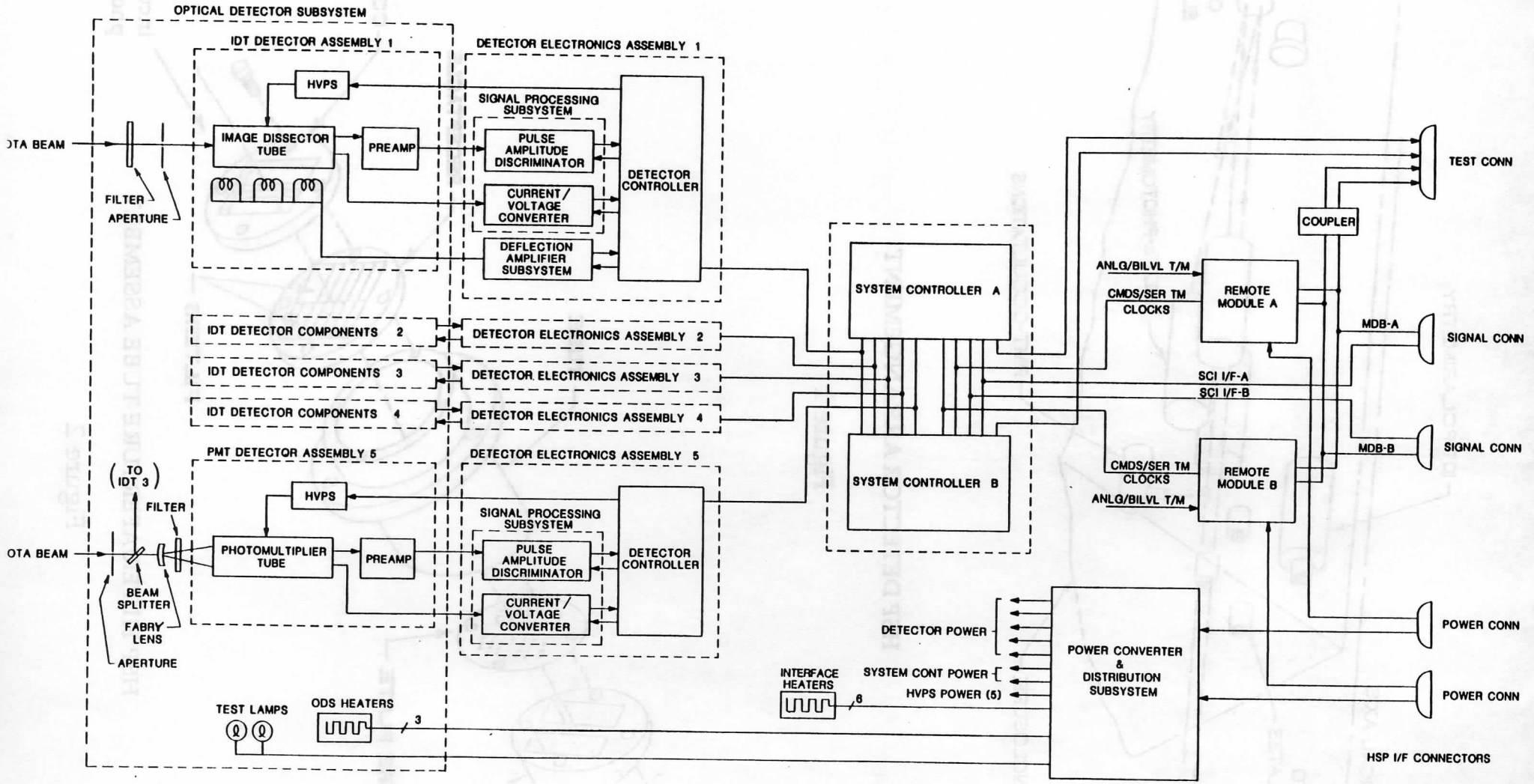

Figure 3

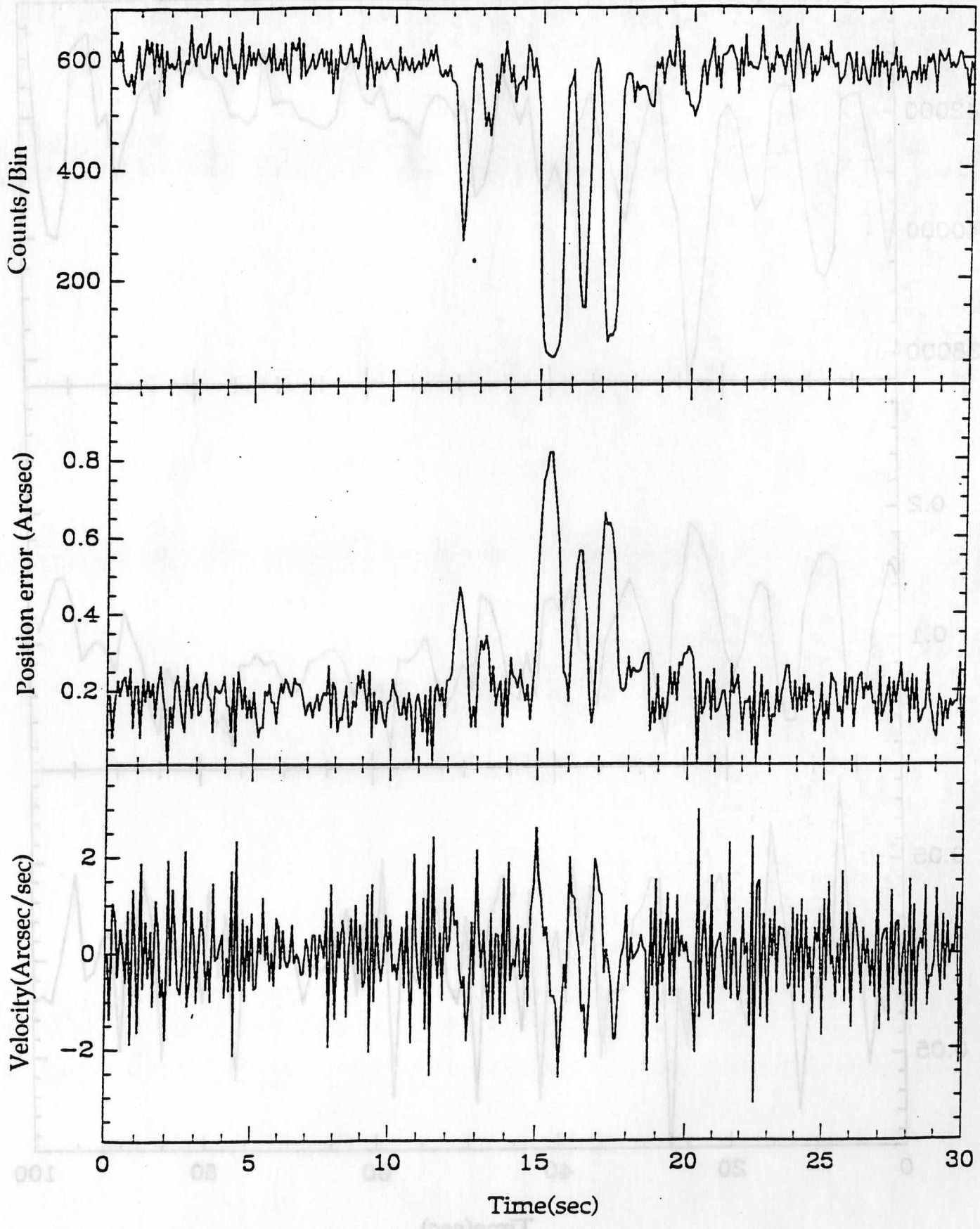
Counts/Bin
600
400
200
Position error (Arcsec)
0.8
0.6
0.4
0.2
Velocity(Arcsec/sec)
2
0
−2
0
5
10
15
20
25
30
Time(sec)

Figure 4

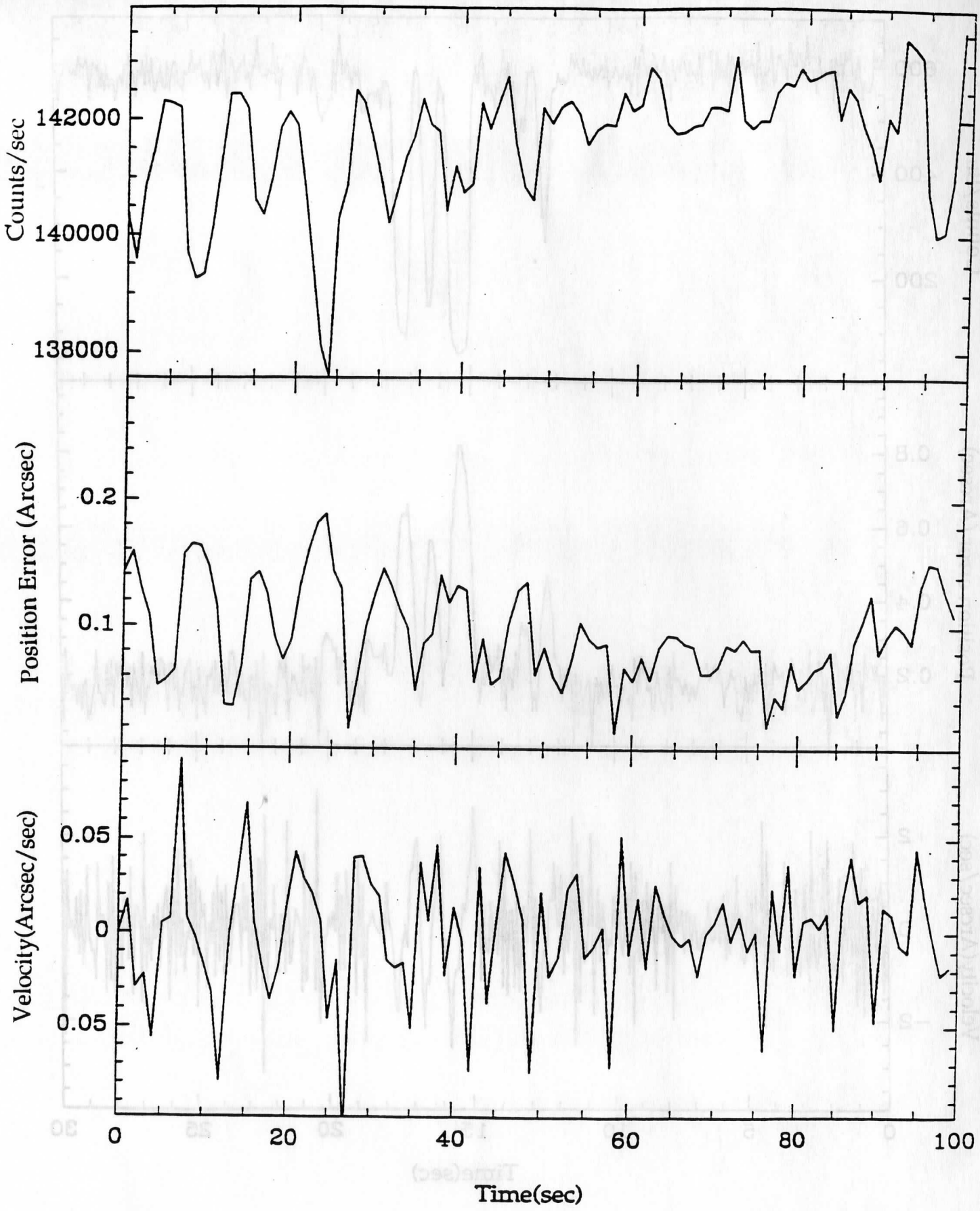
Counts/sec
142000
140000
138000
Position Error (Arcsec)
0.2
0.1
Velocity(Arcsec/sec)
0.05
0
0.05
0
20
40
60
80
100
Time(sec)

Figure 5

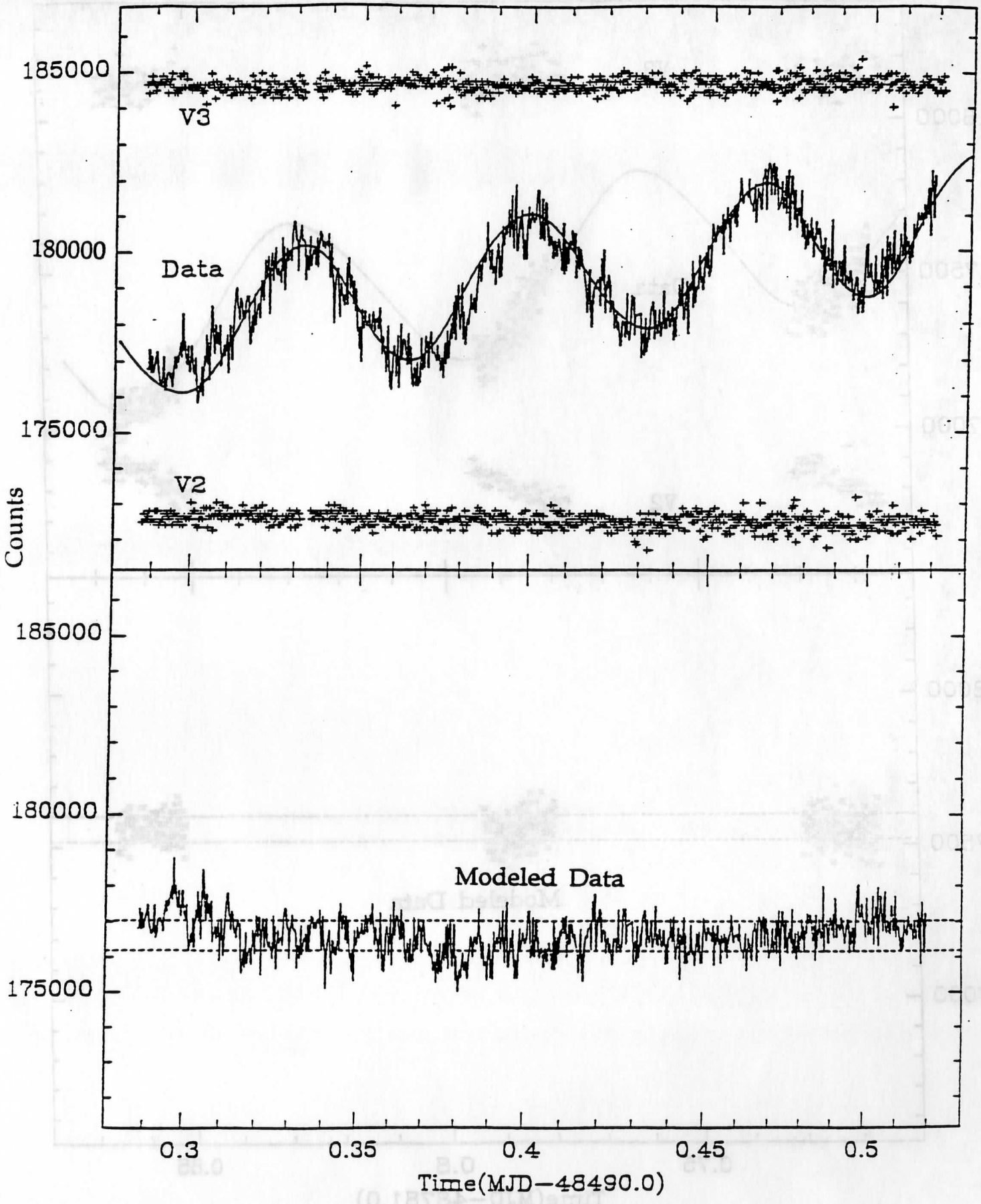
185000
V3
180000
Data
175000
V2
Counts
185000
180000
Modeled Data
175000
0.3
0.35
0.4
0.45
0.5
Time(MJD−48490.0)

Figure 6

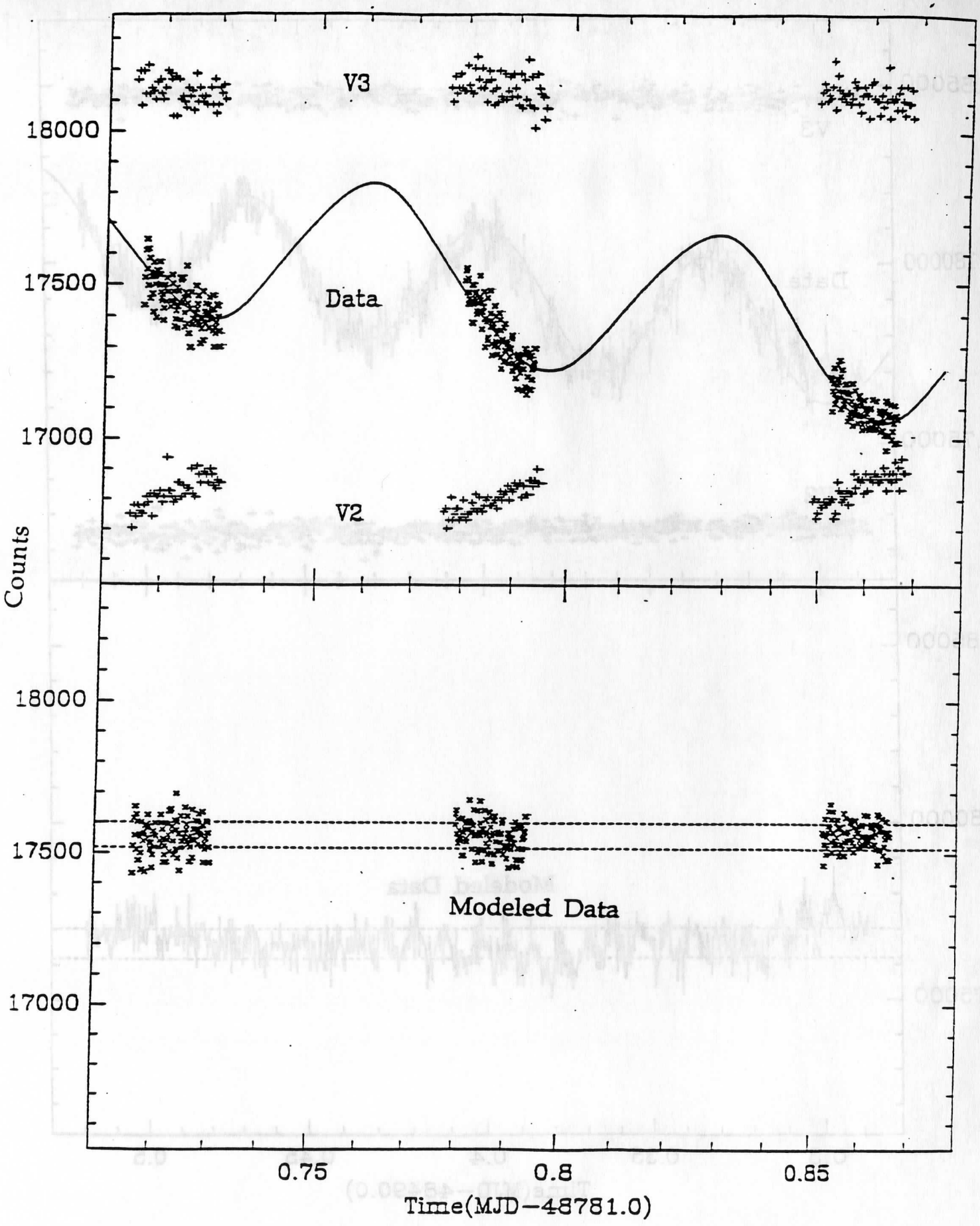
V3
18000
17500
Data
17000
V2
Counts
18000
17500
Modeled Data
17000
0.75
0.8
0.85
Time(MJD−48781.0)

Figure 7

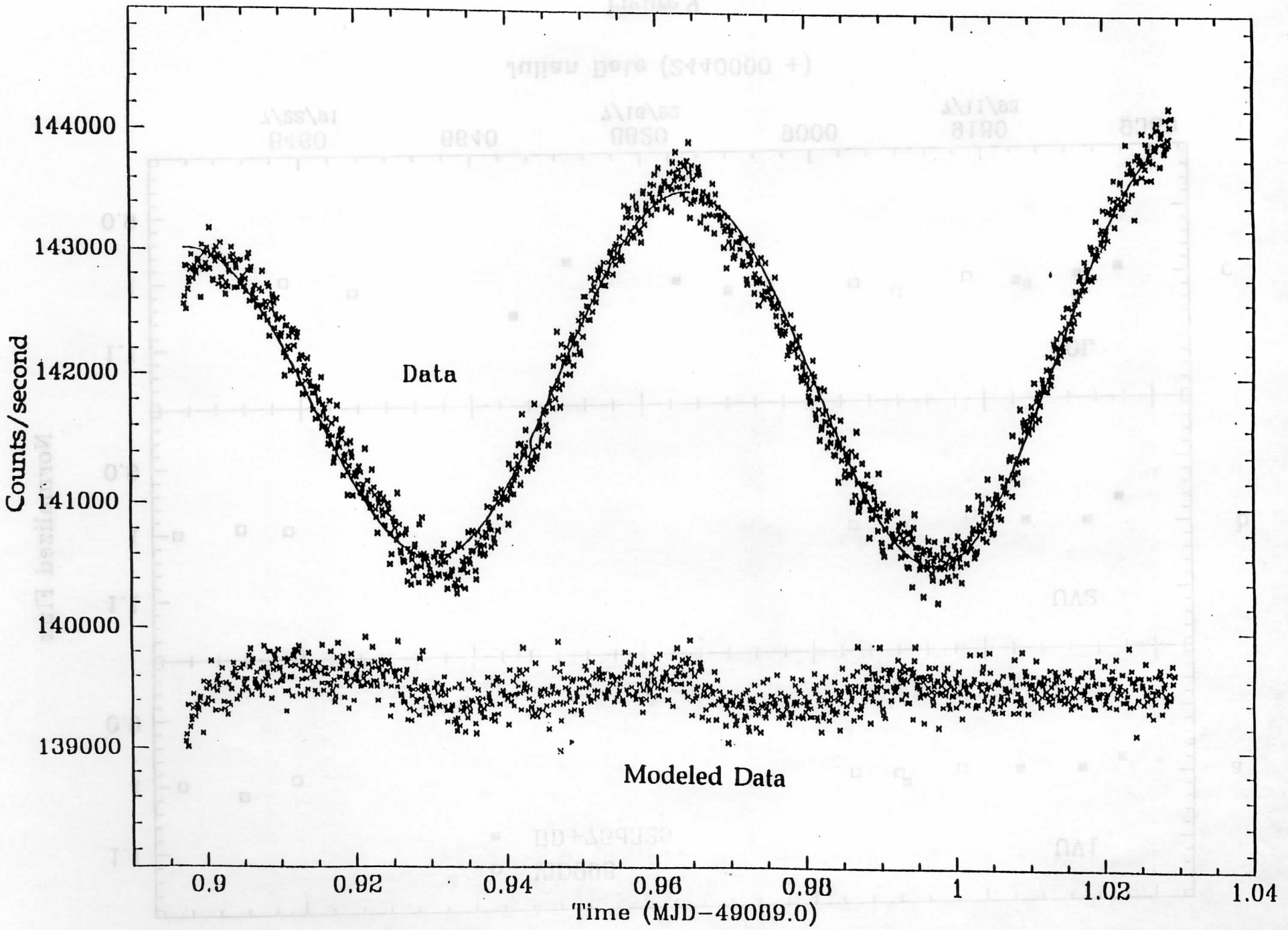
144000
143000
142000
141000
140000
139000
Counts/second
Data
Modeled Data
0.9
0.92
0.94
0.96
0.98
1
1.02
1.04
Time (MJD−49089.0)

Figure 8

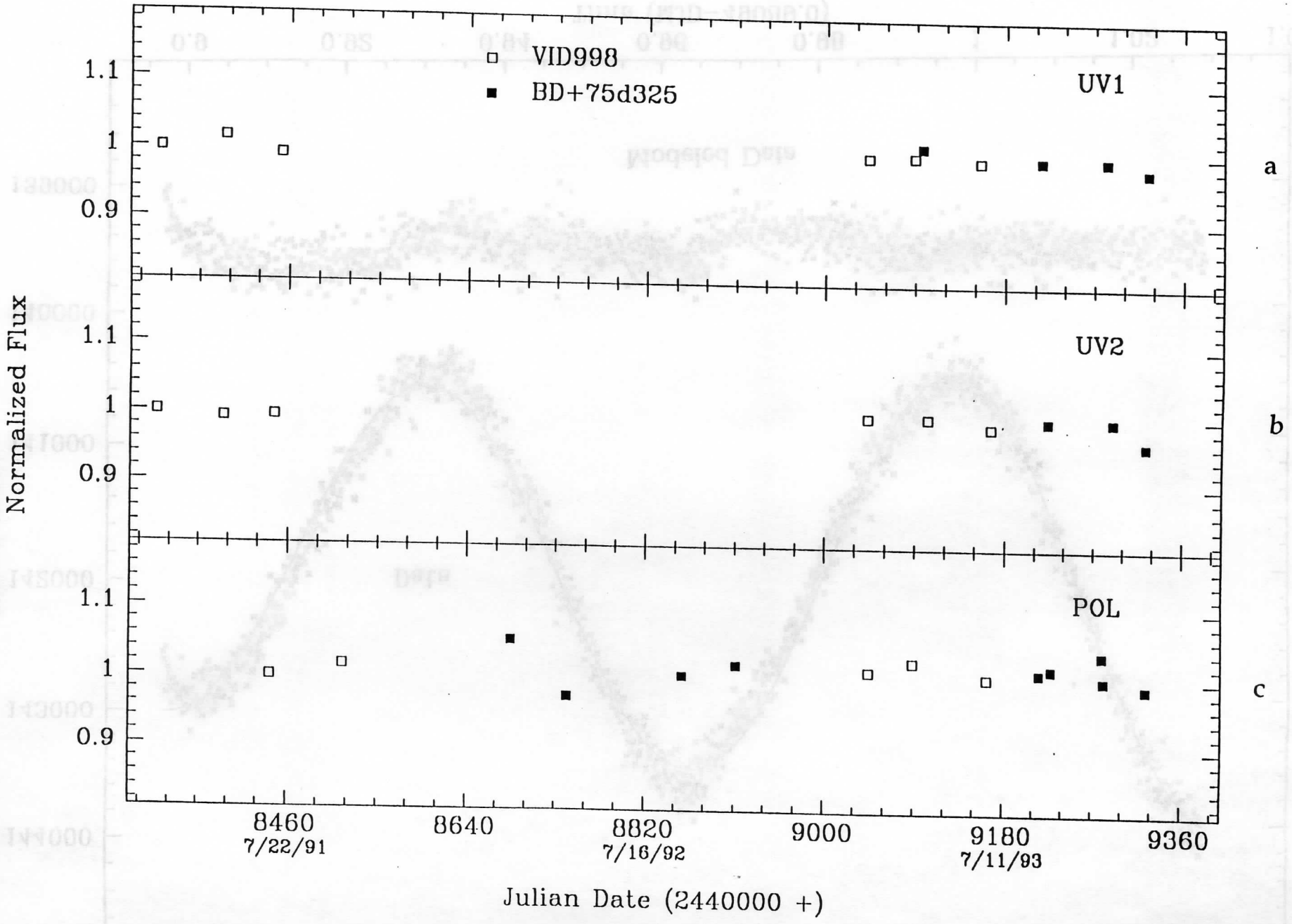
VID998
BD+75d325
UV1
UV2
POL
a
b
c
Normalized Flux
1.1
1
0.9
8460
7/22/91
8640
8820
7/16/92
9000
9180
7/11/93
9360
Julian Date (2440000 +)

Figure 9

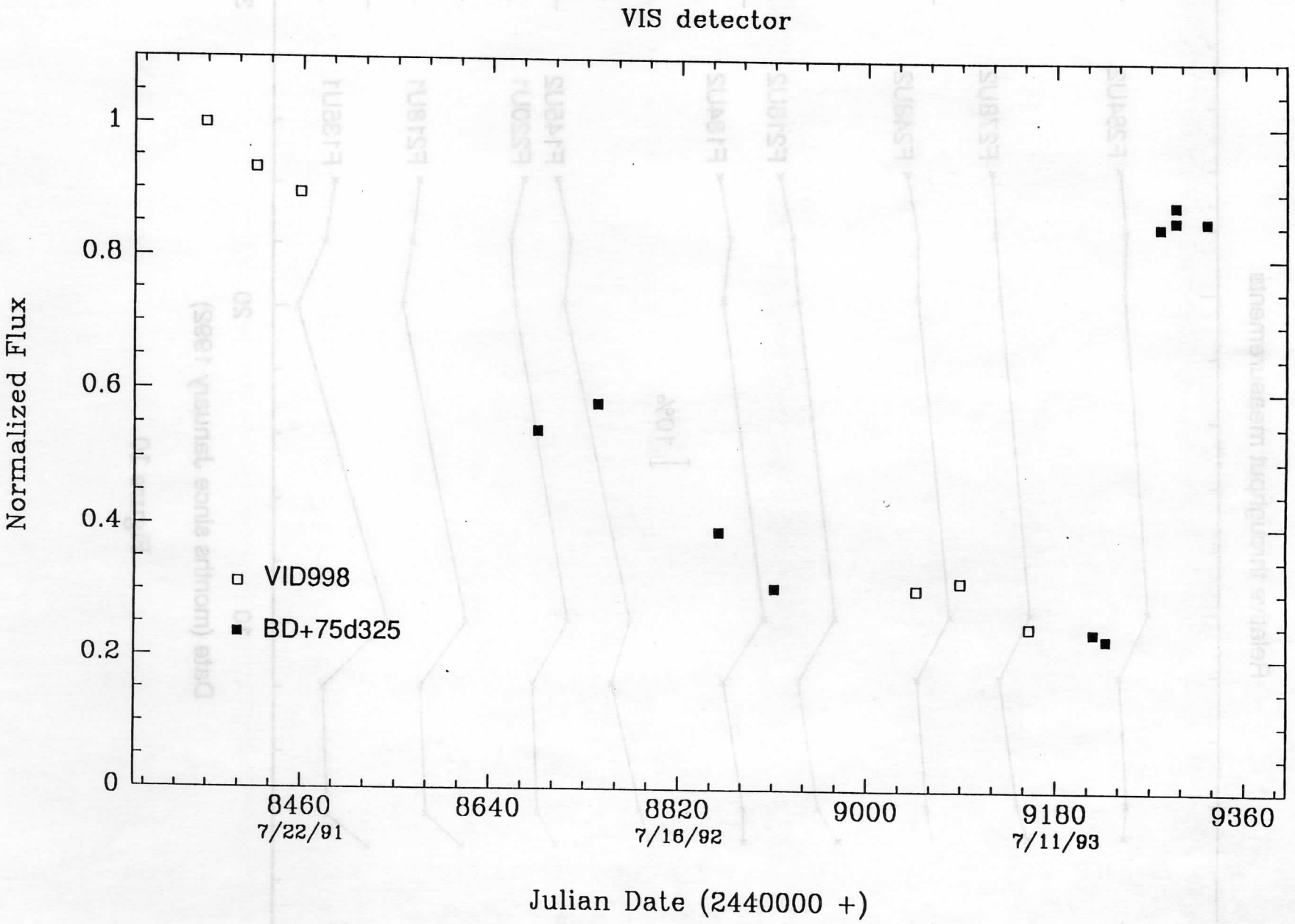
VIS detector
Normalized Flux
1
0.8
0.6
0.4
0.2
0
VID998
BD+75d325
8460
7/22/91
8640
8820
7/16/92
9000
9180
7/11/93
9360
Julian Date (2440000 +)

Figure 9d

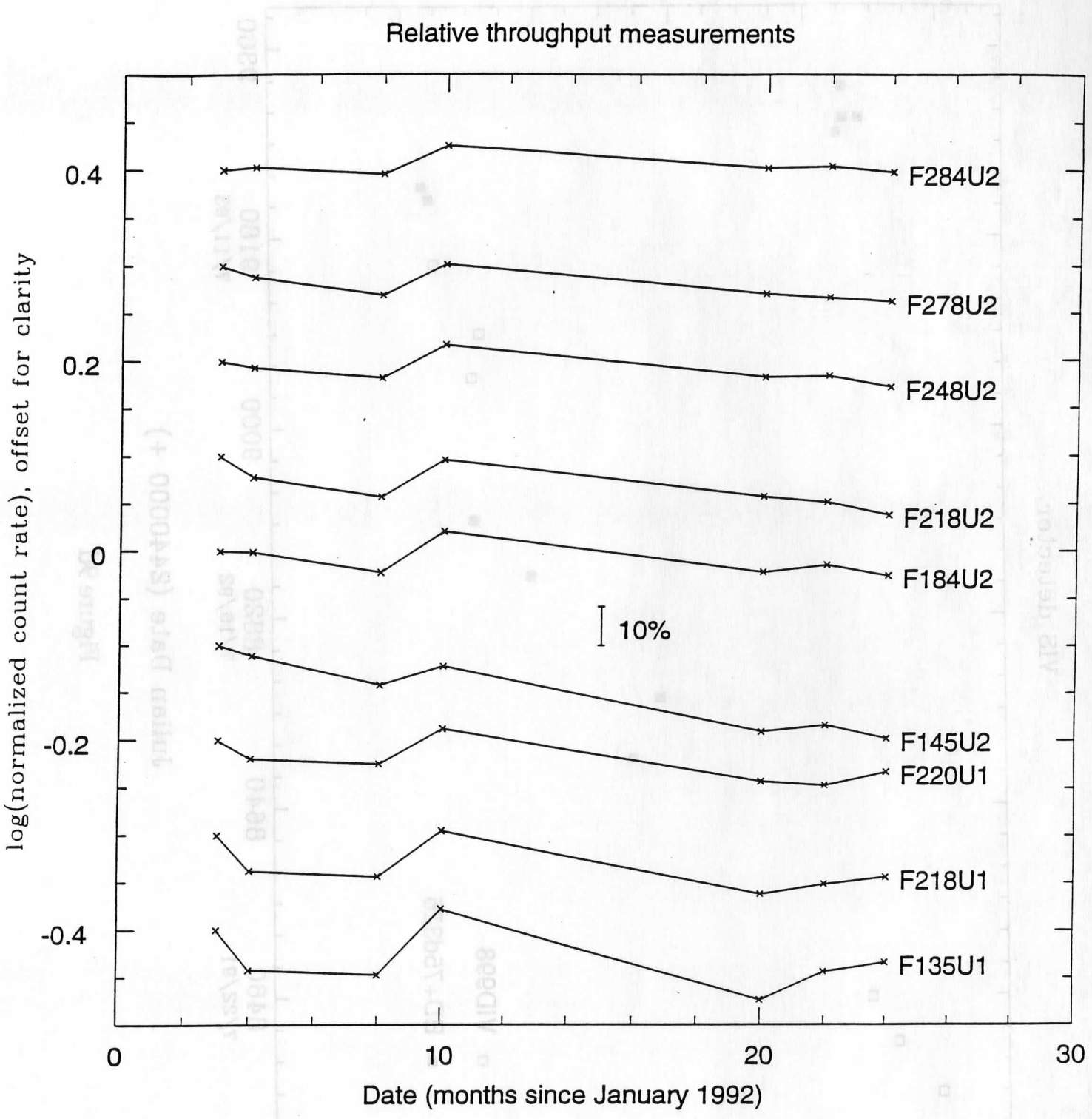
Relative throughput measurements
0.4
0.2
0
-0.2
-0.4
log(normalized count rate), offset for clarity
F284U2
F278U2
F248U2
F218U2
F184U2
10%
F145U2
F220U1
F218U1
F135U1
0
10
20
30
Date (months since January 1992)

Figure 10

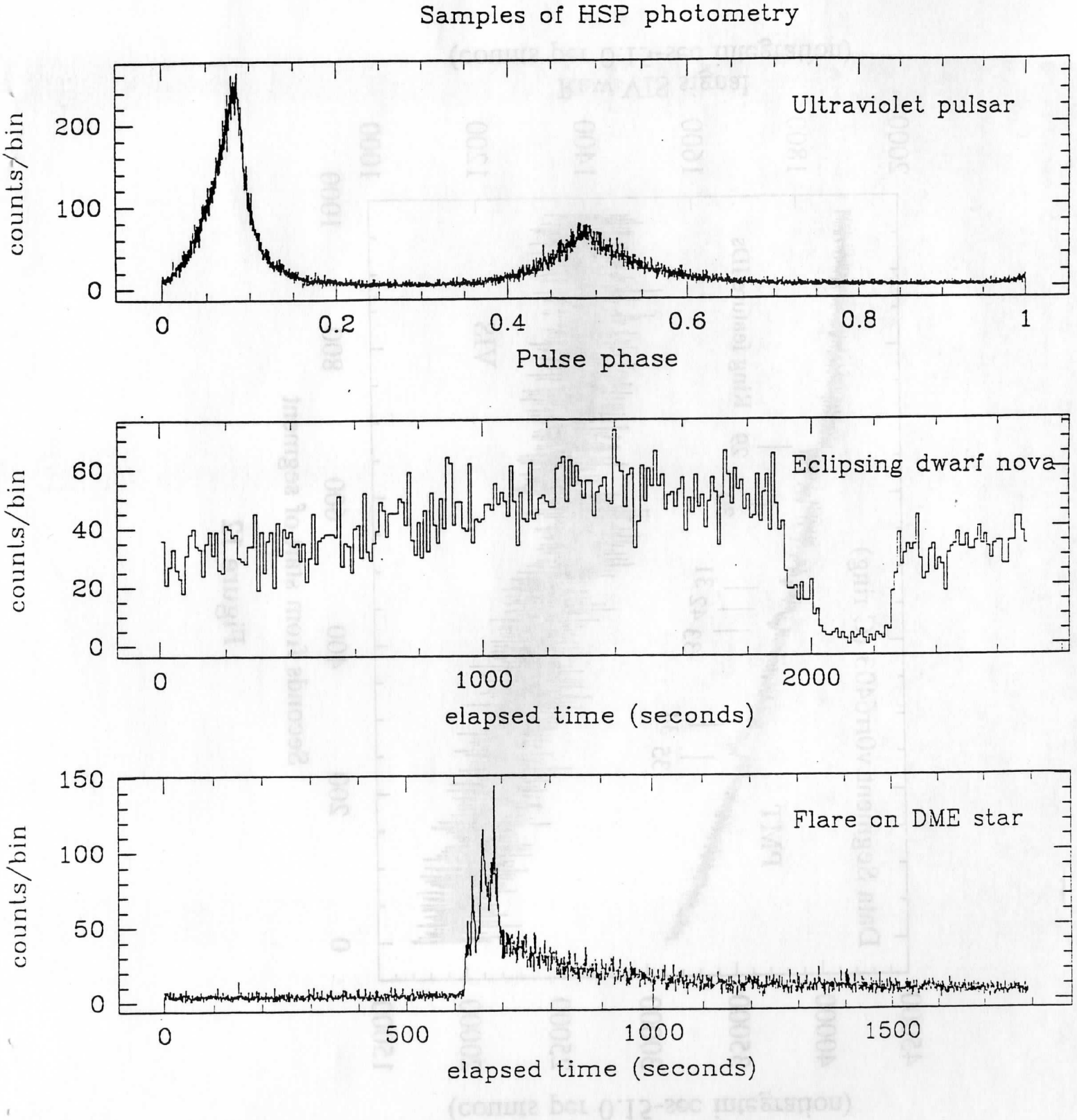
Samples of HSP photometry
Ultraviolet pulsar
counts/bin
200
100
0
0
0.2
0.4
0.6
0.8
1
Pulse phase
Eclipsing dwarf nova
counts/bin
60
40
20
0
0
1000
2000
elapsed time (seconds)
Flare on DME star
counts/bin
150
100
50
0
0
500
1000
1500
elapsed time (seconds)

Figure 11

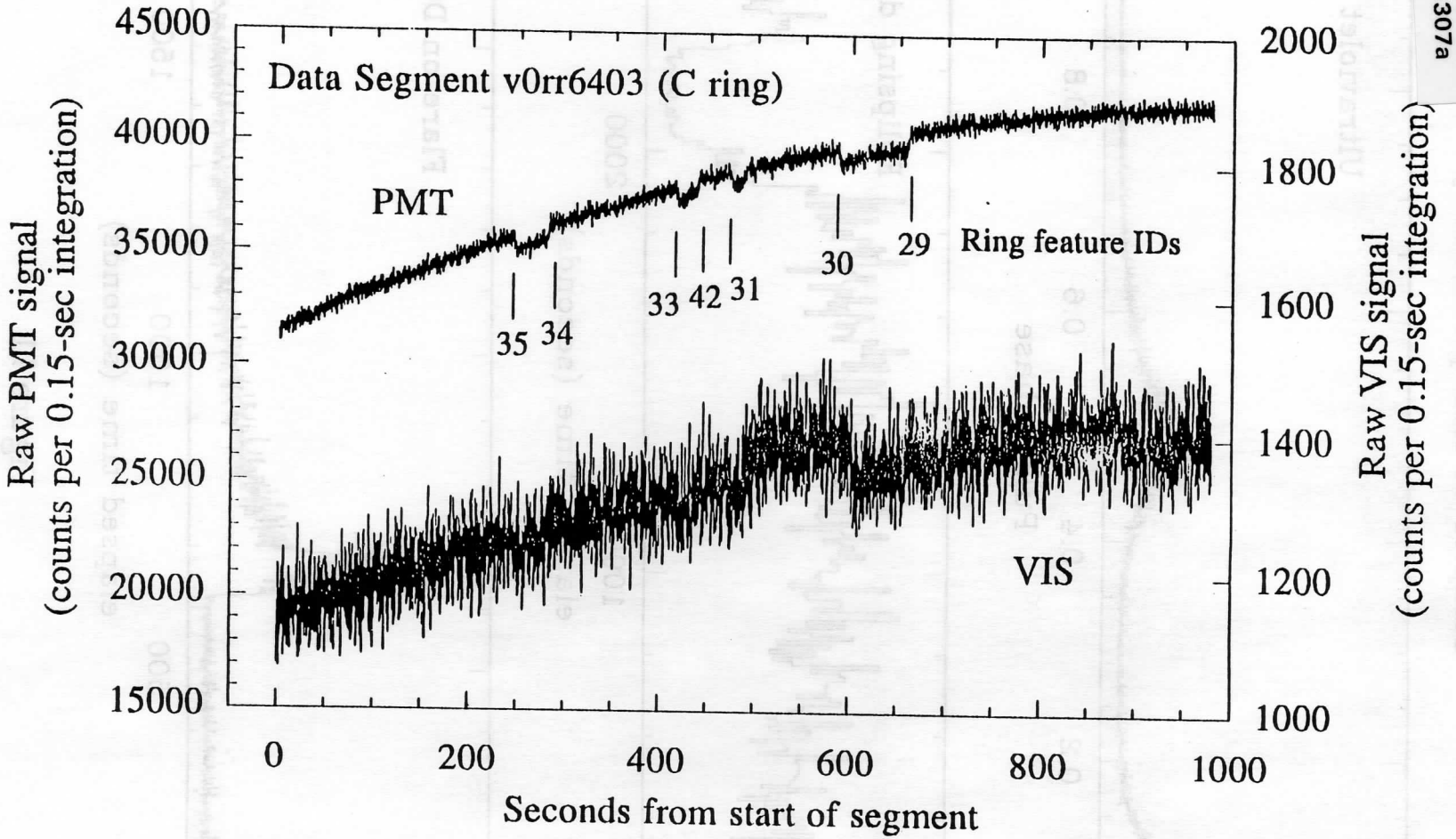
Data Segment v0rr6403 (C ring)
PMT
VIS
Ring feature IDs
35
34
33
42
31
30
29
Raw PMT signal
(counts per 0.15-sec integration)
Raw VIS signal
(counts per 0.15-sec integration)
Seconds from start of segment
45000
40000
35000
30000
25000
20000
15000
2000
1800
1600
1400
1200
1000
0
200
400
600
800
1000

Figure 12